EUROPEAN LABORATORY FOR PARTICLE PHYSICS

July 2, 2008

Status Report to the proposal P330

Calibration and Analysis of the 2007 Data

By NA61 Collaboration
http://na61.web.cern.ch

CERN-SPSC-2008-018 / SPSC-SR-033
03/07/2008

Abstract

The physics program of the NA61/SHINE (SHINE ≡ SPS Heavy Ion and Neutrino Experiment) experiment at the CERN SPS consists of three subjects. In the first stage of data taking (2007-2009) measurements of hadron production in hadron-nucleus interactions needed for neutrino (T2K) and cosmic-ray (Pierre Auger and KASCADE) experiments will be performed. In the second stage (2009-2010) hadron production in proton-proton and proton-nucleus interactions needed as reference data for a better understanding of nucleus-nucleus reactions will be studied. In the third stage (2009-2013) energy dependence of hadron production properties will be measured in p+p, p+Pb interactions and nucleus-nucleus collisions, with the aim to identify the properties of the onset of deconfinement and find evidence for the critical point of strongly interacting matter.

The NA61 experiment was approved at CERN in June 2007. The first pilot run was performed during October 2007. Calibrations of all detector components have been performed successfully and preliminary uncorrected spectra have been obtained. High quality of track reconstruction and particle identification similar to NA49 has been achieved. The data and new detailed simulations confirm that the NA61 detector acceptance and particle identification capabilities cover the phase space required by the T2K experiment. This document reports on the progress made in the calibration and analysis of the 2007 data.

The NA61/SHINE Collaboration

N. Abgrall[22], A. Aduszkiewicz[23], B. Andrieu[11], T. Anticic[13], N. Antoniou[18], A. G. Asryan[15], B. Baatar[9], A. Blondel[22], J. Blumer[5], L. Boldizsar[10], A. Bravar[22], J. Brzychczyk[8], S. A. Bunyatov[9], K.-U. Choi[12], P. Christakoglou[18], P. Chung[16], J. Cleymans[1], D. A. Derkach[15], F. Diakonos[18], W. Dominik[23], J. Dumarchez[11], R. Engel[5], A. Ereditato[20], G. A. Feofilov[15], Z. Fodor[10], M. Gaździcki[17,21], M. Golubeva[6], K. Grebieszkow[24], F. Guber[6], T. Hasegawa[7], A. Haungs[5], M. Hess[20], S. Igolkin[15], A. S. Ivanov[15], A. Ivashkin[6], K. Kadija[13], N. Katrynska[8], D. Kielczewska[23], D. Kikola[24], J.-H. Kim[12], T. Kobayashi[7], V. I. Kolesnikov[9], D. Kolev[4], R. S. Kolevatov[15], V. P. Kondratiev[15], A. Kurepin[6], R. Lacey[16], A. Laszlo[10], S. Lehmann[20], B. Lungwitz[21], V. V. Lyubushkin[9], A. Maevskaya[6], Z. Majka[8], A. I. Malakhov[9], A. Marchionni[2], A. Marcinek[8], M. Di Marco[22], I. Mariş[5], V. Matveev[6], G. L. Melkumov[9], A. Meregaglia[2], M. Messina[20], C. Meurer[5], P. Mijakowski[14], M. Mitrovski[21], T. Montaruli[18,*], St. Mrówczyński[17], S. Murphy[22], T. Nakadaira[7], P. A. Naumenko[15], V. Nikolic[13], K. Nishikawa[7], T. Palczewski[14], G. Palla[10], A. D. Panagiotou[18], W. Peryt[24], A. Petridis[18], R. Planeta[8], J. Pluta[24], B. A. Popov[9,11], M. Posiadala[23], P. Przewlocki[14], W. Rauch[3], M. Ravonel[22], R. Renfordt[21], D. Röhrich[19], E. Rondio[14], B. Rossi[20], M. Roth[5], A. Rubbia[2], M. Rybczynski[17], A. Sadovsky[6], K. Sakashita[7], T. Schuster[21], T. Sekiguchi[7], P. Seyboth[17], K. Shileev[6], A. N. Sissakian[9], E. Skrzypczak[23], M. Slodkowski[24], A. S. Sorin[9], P. Staszel[8], G. Stefanek[17], J. Stepaniak[14], C. Strabel[2], H. Stroebele[21], T. Susa[13], I. Szentpetery[10], M. Szuba[24], A. Taranenko[16], R. Tsenov[4], R. Ulrich[5], M. Unger[5], M. Vassiliou[18], V. V. Vechernin[15], G. Vesztergombi[10], Z. Wlodarczyk[17], A. Wojtaszek[17], J.-G. Yi[12], I.-K. Yoo[12]

[1]Cape Town University, Cape Town, South Africa
[2]ETH, Zurich, Switzerland
[3]Fachhochschule Frankfurt, Frankfurt, Germany
[4]Faculty of Physics, University of Sofia, Sofia, Bulgaria
[5]Forschungszentrum Karlsruhe, Karlsruhe, Germany
[6]Institute for Nuclear Research, Moscow, Russia
[7]Institute for Particle and Nuclear Studies, KEK, Tsukuba, Japan
[8]Jagellionian University, Cracow, Poland
[9]Joint Institute for Nuclear Research, Dubna, Russia
[10]KFKI Research Institute for Particle and Nuclear Physics, Budapest, Hungary
[11]LPNHE, University of Paris VI and VII, Paris, France
[12]Pusan National University, Pusan, Republic of Korea
[13]Rudjer Boskovic Institute, Zagreb, Croatia
[14]Soltan Institute for Nuclear Studies, Warsaw, Poland
[15]St. Petersburg State University, St. Petersburg, Russia
[16]State University of New York, Stony Brook, USA
[17]Świ etokrzyska Academy, Kielce, Poland
[18]University of Athens, Athens, Greece
[19]University of Bergen, Bergen, Norway
[20]University of Bern, Bern, Switzerland
[21]University of Frankfurt, Frankfurt, Germany
[22]University of Geneva, Geneva, Switzerland
[23]University of Warsaw, Warsaw, Poland
[24]Warsaw University of Technology, Warsaw, Poland

1 Introduction

The physics program of the NA61/SHINE (SHINE ≡ SPS Heavy Ion and Neutrino Experiment) experiment at the CERN SPS [1, 2, 3] consists of three main subjects. In the first stage of data taking (2007-2009) measurements of hadron production in hadron-nucleus interactions needed for neutrino (T2K) and cosmic-ray (Pierre Auger and KASCADE) experiments will be performed. In the second stage (2009-2011) hadron production in proton-proton and proton-nucleus interactions needed as reference data for a better understanding of nucleus-nucleus reactions will be studied. In the third stage (2009-2013) energy dependence of hadron production properties will be measured in p+p and p+Pb interactions as well as in nucleus-nucleus collisions, with the aim to identify the properties of the onset of deconfinement and find evidence for the critical point of strongly interacting matter.

The experiment was approved at CERN in June 2007. The first pilot run was performed during October 2007. The aims of this run were [2]:

- to set up and test the NA61/SHINE apparatus and the detector prototypes,
- to take pilot physics data on interactions of 31 GeV/c protons on a thin carbon and the T2K replica targets.

This document presents a status report on the calibration and analysis of the pilot data taken in the 2007 October run of NA61.

2 The NA61/SHINE detector

The NA61/SHINE experiment is a large acceptance hadron spectrometer at the CERN-SPS for the study of the hadronic final states produced in interactions of various beam particles (π, p, C, S and In) with a variety of fixed targets at the SPS energies. The layout of the NA61/SHINE set-up is shown in Fig. 1. The main components of the current detector were constructed and used by the NA49 experiment [4]. The main tracking devices are four large volume Time Projection Chambers (TPCs), see Fig. 1, which are capable of detecting up to 70% of all charged particles created in the reactions studied. Two of them, the vertex TPCs (VTPC-1 and VTPC-2), are located in the magnetic field of two super-conducting dipole magnets (maximum bending power of 9 Tm) and two others (MTPC-L and MTPC-R) are positioned downstream of the magnets symmetrically with respect to the beam line. One additional small TPC, the so-called gap TPC (GTPC), is installed on the beam axis between the vertex TPCs. The setup is supplemented by time of flight detector arrays two of which (ToF-L/R) were inherited from NA49 and can provide a time measurement resolution of $\sigma_{tof} \approx 60$ ps.

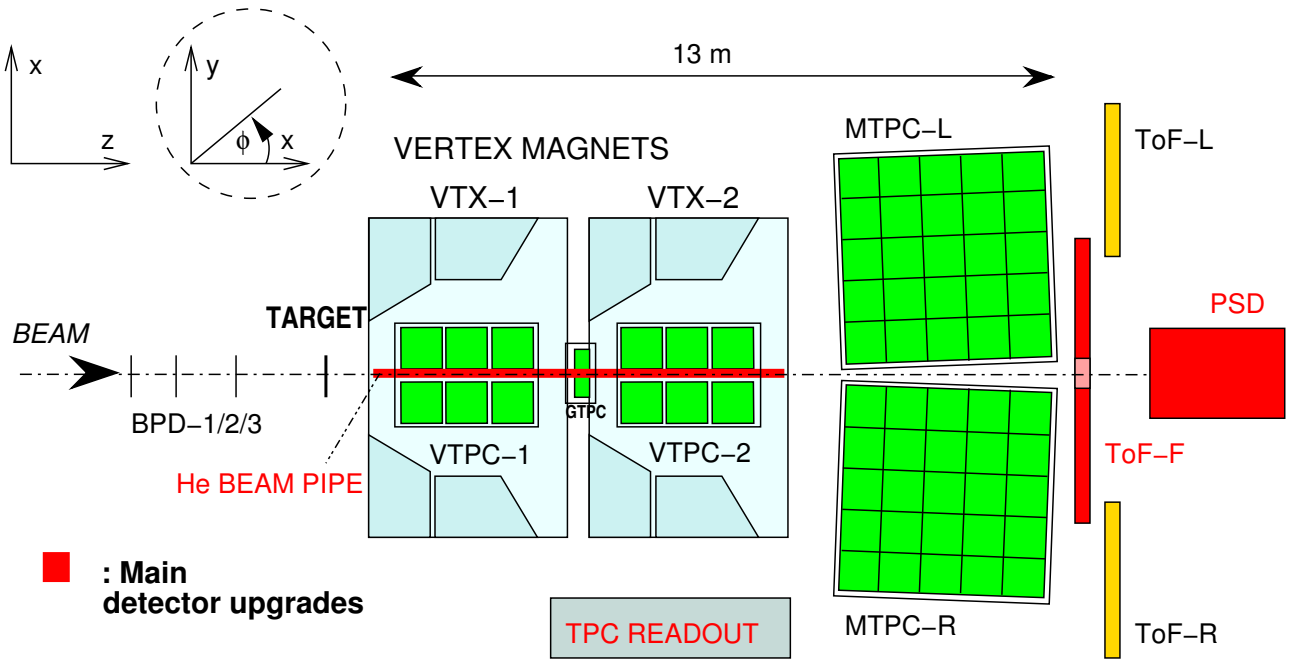

Figure 1: The layout of the NA61/SHINE set-up (top view, not to scale) with the basic upgrades indicated in red.

For the 2007 run a new forward time of flight detector (ToF-F) was constructed in order to extend the acceptance of the NA61/SHINE set-up for pion and kaon identification as required for the T2K measurements. The ToF-F detector consists of 64 scintillator bars, oriented vertically, and read out on both sides with Hamamatsu R1828 photo-multipliers. The size of each scintillator bar is $120 \times 10 \times 2.5$ cm^3. The expected resolution of the new ToF-F wall is ≤ 120 ps. This resolution provides a 5 σ π/K separation at 3 GeV/c. The ToF-F wall is installed downstream of the MTPC-L and MTPC-R (see Fig. 1), closing the gap between the ToF-R and ToF-L walls.

Furthermore, numerous small modifications and upgrades of the NA61/SHINE facility were performed before the 2007 run. They include:

- speed-up of the ToF-L/R readout,
- modification of the DAQ system to allow writing data on disk,
- refurbishing of the Beam Position Detectors (BPD-1/2/3 in Fig. 1),
- preparation of the targets and target holders and
- preparation and installation of the new beam counters for a new trigger logic.

Two carbon (isotropic graphite) targets were used during the 2007 run:

- a 2 cm-long target (about 4% of a nuclear interaction length, λ_{I}) with density $\rho = 1.84$ g/cm^3, the so-called thin target,
- a 90 cm long cylinder of 2.6 cm diameter (about 1.9 λ_{I}), the so-called T2K replica target with density $\rho = 1.83$ g/cm^3.

The center of the targets was positioned about 80 cm upstream from the VTPC-1 entrance window.

Proton beam particles are identified and selected by means of CEDAR-West and threshold Cerenkov counters as well as several scintillation counters. The trajectory of beam particles is precisely measured by the BPDs. These detectors consist of pairs of proportional chambers and are positioned along the beam line.

Interactions in the target were selected by an anti-coincidence of the incoming beam particle with a small scintillation counter (S4) placed on the beam axis between the two vertex magnets.

Two detector prototypes were constructed for and tested during the 2007 run, namely:

- the super-module of the Projectile Spectator Detector (PSD) [5] and
- the "FE Tester" needed for the development of the new TPC readout electronics.

3 The 2007 run and the registered data

The 2007 NA61/SHINE pilot run started on September 27 and ended on October 29. During this period the following studies were performed:

- September 27 - October 3:
  test of the PSD super-module with beams of muons at 75 GeV/c and hadrons at 20, 30, 40, 80 and 158 GeV/c;
- September 27 - October 12:
  installation, test and tuning of the beam and trigger counters with beams of hadrons at 75 GeV/c and 31 GeV/c; optimization of the proton beam at 31 GeV/c;
- October 13 - October 24:
  pilot data taking with 31 GeV/c protons on the thin graphite target;
- October 25 - October 29:
  pilot data taking with 31 GeV/c protons on the T2K replica graphite target;
- October 25 - October 29:
  TPC readout tests with the "FE Tester".

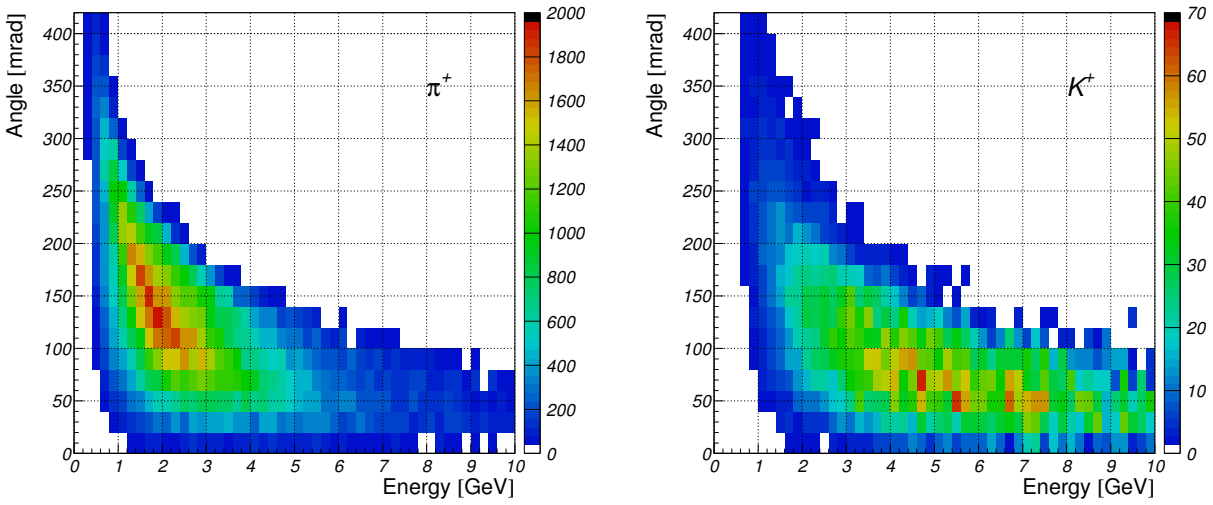

Figure 2: Simulated distributions of pions (left) and kaons (right) whose daughter neutrinos pass through the Super-Kamiokande detector. The spectra are plotted as a function of the polar angle and energy in the laboratory.

In total about 1.5×10^6 events were registered for the NA61 physics programme. This includes about 670 k events with the thin target, 230 k events with the T2K replica target and 80 k events without target (empty target events).

The NA61/SHINE software has been set up and tested on the 2007 data. Both reconstruction and simulation chains have been heavily used for the on-line and off-line quality control as well as for the acceptance studies. The data taken during the 2007 run have been processed several times to perform detector calibration and to obtain first preliminary physics results.

4 Goals of the 2007 data analysis

The main motivation and goal of the analysis of the 2007 data is to obtain the inclusive spectra of pions and kaons produced in p+C interactions at 31 GeV/c and emitted from the T2K replica target. This will allow the absolute determination of the neutrino flux of the T2K long baseline neutrino oscillation experiment at J-PARC [6]. The required acceptance of the hadron production measurements for T2K is shown in Fig. 2 for pions and kaons separately. The uncertainties in particle production at the T2K target lead to important uncertainties in the oscillation analysis. Furthermore, they preclude precise measurements of neutrino inclusive and exclusive cross-sections.

The T2K experiment is expected to probe $\nu_\mu \rightarrow \nu_e$ oscillation down to an order of magnitude better than the current bound. This goal requires a systematic error of less than 10% on the prediction of background events (including systematics from the far to near ratio, measurements at the near detector, cross-sections and detection efficiencies). Monte Carlo studies showed that an error of the order of 2-3% on the far to near ratio would significantly constrain the error on the background over the region of interest (neutrino energy between 0 and 1 GeV). The same requirement has been determined for the ν_μ disappearance channel.

To estimate the required accuracy to achieve a precision of 2-3% on the far to near ratio, a 10% error on hadroproduction rates in each momentum-angle bin of the T2K phase space (200 MeV$\times$20 mrad) has been applied. This implies a $\delta R_{\mu,e} \sim 1\%$ over 0-1 GeV, which is actually better than the required precision. Measurements with 10% accuracy require 100 tracks per bin, which means $\sim$ 200 k tracks in the T2K phase space. Since this phase space accounts only for 20% of the NA61 acceptance, 1 M tracks would in principle be necessary.

Measurements of hadro-production at NA61 within 10% accuracy will allow the determination of the far to near ratio at the level of 2-3% precision. This in turn will constrain enough the systematic errors to allow considerable improvement in the T2K physics achievements.

The NA61 measurements of hadron production in p+C interactions at 31 GeV/c will also be valuable for cosmic-ray physics and for the physics of strong interactions [1].

5 Organization and manpower

The organization of and manpower involved in the calibration and analysis of the data registered in the 2007 run followed closely the plan formulated in Addendum-2 [3] to the NA61 proposal. Groups with different physics priorities and experience in the NA49/61 detector/calibration/analysis have been efficiently collaborating in this effort.

The status of the work has been reviewed and next steps were planned during:

- weekly EVO meetings on the software and calibration,
- weekly EVO meetings on the analysis,
- two analysis meetings organized in Warsaw and at CERN and
- two collaboration meetings organized at CERN.

The material shown at the meetings is stored at the NA61 INDICO pages `http://indico.cern.ch/categoryDisplay.py?categId=1471`.

The manpower actively involved in the software, calibration and analysis effort corresponds to the plan presented in Addendum-2 [3].

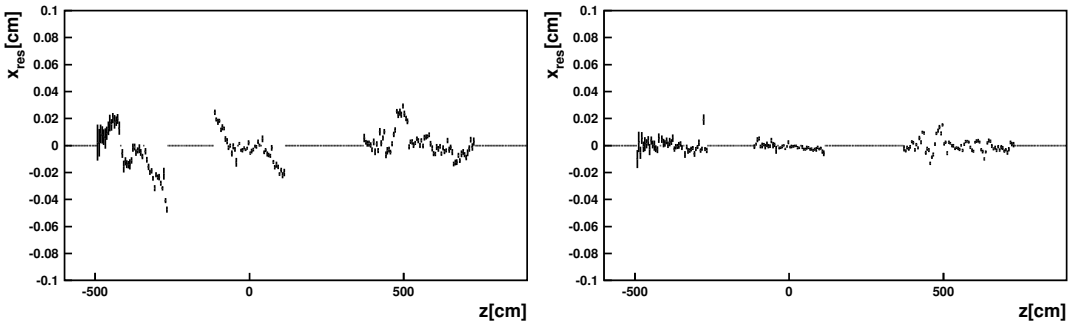

Figure 3: Residuals in the horizontal (x) direction for the TPC points before (left) and after (right) drift velocity and residual corrections are applied.

6 Data calibration and quality assessment

The calibration procedure of the NA61 data is largely based on the approach developed for the NA49 data and consists of numerous steps resulting in optimized parameters for:

- detector geometry, drift velocity and residual corrections,
- magnetic field,
- time of flight measurements and
- specific energy loss measurements.

Each step involves reconstruction of the data required to optimize a given set of calibration constants followed by optimization and verification procedures.

6.1 Detector geometry, drift velocity and residual corrections

The optimization of the detector geometry, determination of TPC drift velocities and evaluation of the residual corrections of TPC points starts from the geometry parameters measured by the CERN surveyor group and the drift velocities measured by the NA61 drift velocity monitors. In an iterative procedure small corrections to the measured parameters are calculated. These corrections follow from the requirement that deviations (residuals) between the measured points and the fitted track trajectories are minimal. The MILLEPEDE package [7] was used for the minimization purposes.

The largest corrections to the measured parameters were found for the vertical position of the BPD detectors (correction of about +0.4 cm) and for the MTPC-L drift velocity (correction of about +2%). Furthermore, it was also necessary to introduce a time dependent drift velocity

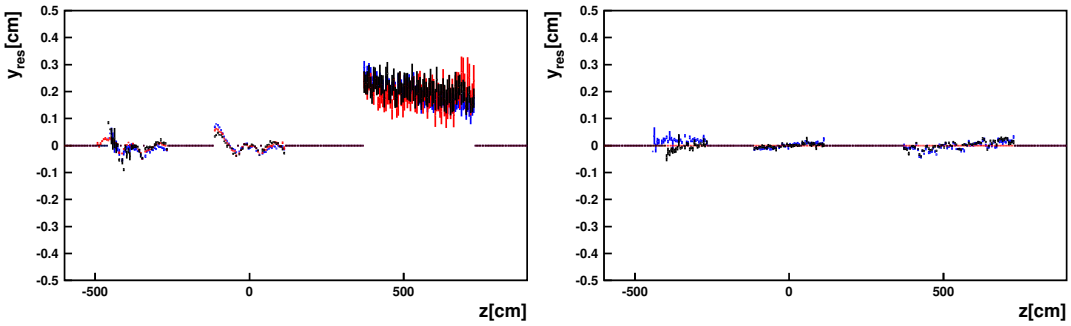

Figure 4: *Left:* Residuals in the vertical (y) direction for the TPC points before drift velocity and residual corrections are applied. Results for points located in the top ($y < 10$ cm), central ($-10 < y < 10$ cm) and bottom ($y < -10$ cm) TPC domains are indicated by black, blue and red color, respectively. *Right:* The same as in the left plot but after the drift velocity and residual corrections.

correction ($\leq 0.2\%$). These 3 corrections were applied before starting the overall optimization procedure based on the MILLEPEDE package.

The mean residuals calculated along the x (magnetic bending) and y (vertical) directions as a function of the z-coordinate of the TPC points (see Fig. 1 for the NA61 coordinate system definition) are shown in Figs. 3 and 4 before and after the calibration procedure, respectively. The calibrated data show deviations which are typically smaller than 200 μm.

For the 2008 run it is planned to optimize the surveying procedure as well as to investigate and improve the time stability and the absolute calibration of the TPC drift velocities. This will significantly reduce the magnitude of the data based corrections as well as simplify and accelerate the calibration procedure.

6.2 Magnetic field calibration

Proper reconstruction of the NA61 data requires precise knowledge of the magnitude and orientation of the magnetic field of the two super-conducting dipole magnets (VTX-1 and VTX-2 in Fig. 1). NA61 uses the field maps calculated by the NA49 Collaboration. This is possible because the magnets and their positions remain unchanged since the beginning of the NA49 operation.

The magnetic field maps were obtained using two independent methods:

- calculations based on the TOSCA code [8] using the known configuration and material of the iron yokes and coils,

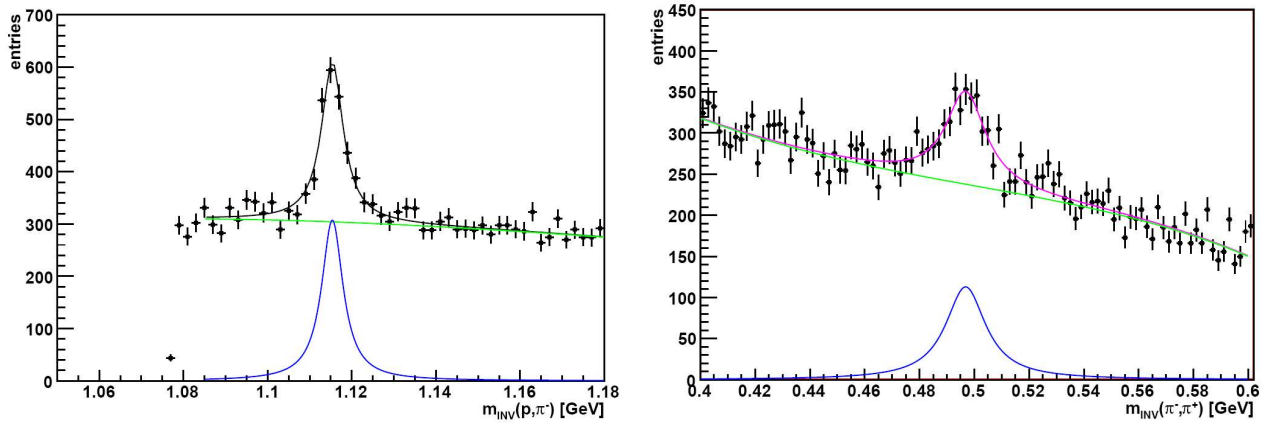

Figure 5: Invariant mass spectra of Λ (left) and K^0_S (right) candidates in p+C interactions registered in the 2007 run. The positions of observed maxima were used to validate the scale factor α of the magnetic field map used in the reconstruction.

- detailed field measurements performed by means of Hall probes on a three dimensional grid with 4 cm $\times$ 4 cm $\times$ 4 cm spacing.

In order to cover the entire sensitive region of the TPCs, the magnetic field measurements extended over about 16.5 m^3. A comparison of the calculated field map with the measurements showed agreement within 0.5%.

In the 2007 run the NA49 nominal magnet currents, which correspond to the field of 1.5 T in VTX-1 and 1.1 T in VTX-2, were scaled by a factor 20/158. During the data taking period the magnitude of the magnetic field was monitored by the reference Hall probes. The NA49 magnetic field which corresponds to the selected current setting was used in the data reconstruction.

Finally the magnetic field map was tested comparing the reconstructed masses of Λ hyperons and K^0_S mesons with the corresponding nominal values. Fig. 5 shows the invariant mass spectra of Λ and K^0_S candidates in p+C interactions at 31 GeV/c registered in the 2007 run. Clear peaks due to Λ and K^0_S decays are observed. The Gauss fit to these peaks yielded reconstructed masses of Λ and K^0_S particles. These masses are plotted in Fig. 6 as a function of the magnetic field scaling factor α. The results demonstrate that the used magnetic field ($\alpha = 1$) yields masses which are consistent with the corresponding nominal values. The statistical resolution of the 2007 data allows to exclude biases larger than 1%.

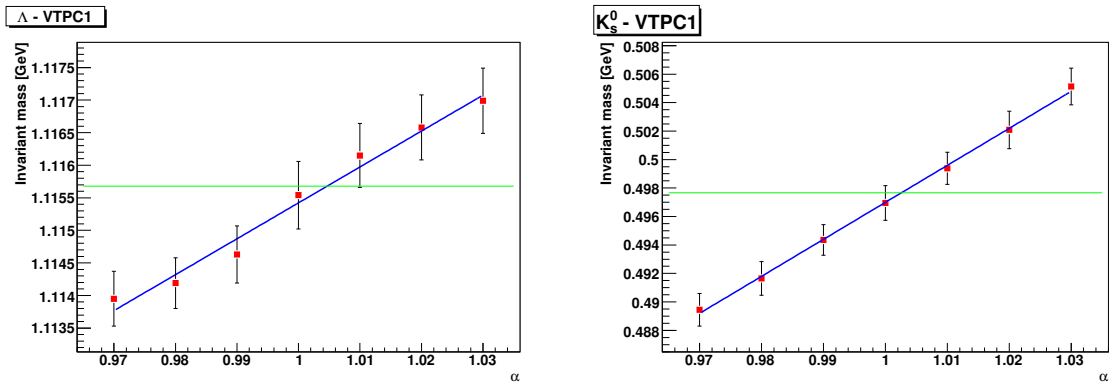

Figure 6: The reconstructed masses of Λ (left) and K^0_S (right) particles as a function of the magnetic field scaling factor α. Dashed horizontal lines indicate the nominal mass values of Λ (left) and K^0_S (right). The magnetic field used by NA61 corresponds to $\alpha = 1$.

6.3 Time of flight measurements

6.3.1 ToF-F calibration

The procedure used for the ToF-F calibration is briefly described below.

Particles hitting a scintillator rod leave a signal in the two corresponding photo-multipliers (PMTs) providing the stop signal for ToF measurement. The start signal is given by the S1 counter positioned upstream of the target (see Fig. 12). The measurement of the time of flight t_{tof} is then carried out by taking the difference in time between the S1 signal and the mean value of the two PMT signals (t_{up} and t_{down}) of the scintillator,

$$t_{tof} = t_{S1} - \frac{t_{up} + t_{down}}{2} + t_0 \ ,$$

where t_0 is a reference time which is specific to each channel as it depends on cable length and PMT gains. Calibrating the ToF-F detector consisted in first associating a hit in a scintillator to a TPC track and second, setting t_0 for all the 128 PMT channels.

A preliminary calibration was performed assuming that above 5 GeV/c all particles had the same time of flight. This calibration allowed to discriminate pions from protons. From then on a refined calibration on a scintillator by scintillator basis was possible by selecting pions only.

The 64 scintillator bars are mounted in such a way that they overlap by 1 cm on either side. A first estimate of the ToF-F resolution is obtained by selecting particles that hit the overlapping region and plotting the time difference between the two scintillator signals as shown in Fig. 7 (left). The Gaussian fit gives a resolution $\sigma_{tof} = \frac{178}{\sqrt{2}} \approx 126$ ps, which is an upper bound considering that the light yield is greatly reduced at the sides of the scintillators.

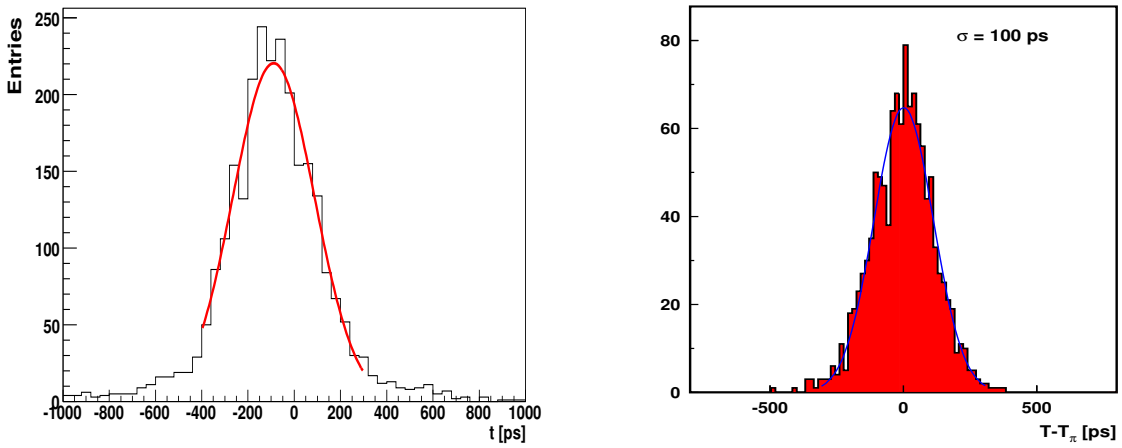

Figure 7: *Left:* Time difference between two overlapping scintillators for the ToF-F detector. The resulting time resolution of a single scintillator measurement is about $\sigma/\sqrt{2} \approx 126$ ps. *Right:* Time differences T-T$_\pi$ for the ToF-L/R system. The width of the distribution provides an estimate of the overall time resolution of about 100 ps.

6.3.2 ToF-L/R calibration

Before the 2007 run the two arrays of the NA61 ToF-L/R detector, each consisting of 891 scintillator pixels positioned on both sides of the beam, were rotated with respect to the vertical axis to allow easy installation and maintenance of the ToF-F system.

The new ToF-L/R geometry was obtained from the data by varying parameters of the ToF wall geometry in all three coordinates and looking for consistency of track projections onto ToF-L/R with signals from the pixels. The accuracy of the pixel position determination is about 3 mm, contributing 15 ps to the final time resolution of the system.

Due to the limited number of track hits per pixel available from the 2007 data sample, the corrections for the dependence of the time-of-flight on signal amplitude and relative position of the hit in each pixel had to be performed using the calibration constants obtained from the last NA49 run period. However, the time offset parameters (T_0 constants), averaged over the entire data taking period, were derived from the 2007 data.

The new S1 scintillation counter, which provides the start signal for the time-of-flight measurements, has an intrinsic time resolution of approximately 60 ps.

The overall time resolution for the ToF-L/R system (averaged over all the pixels) achieved in the 2007 run is demonstrated in Fig. 7 (right) as the difference $T - T_\pi$ between the measured time-of-flight and that calculated assuming the pion mass. The distribution is well fitted by a Gaussian with a standard deviation of 100 ps.

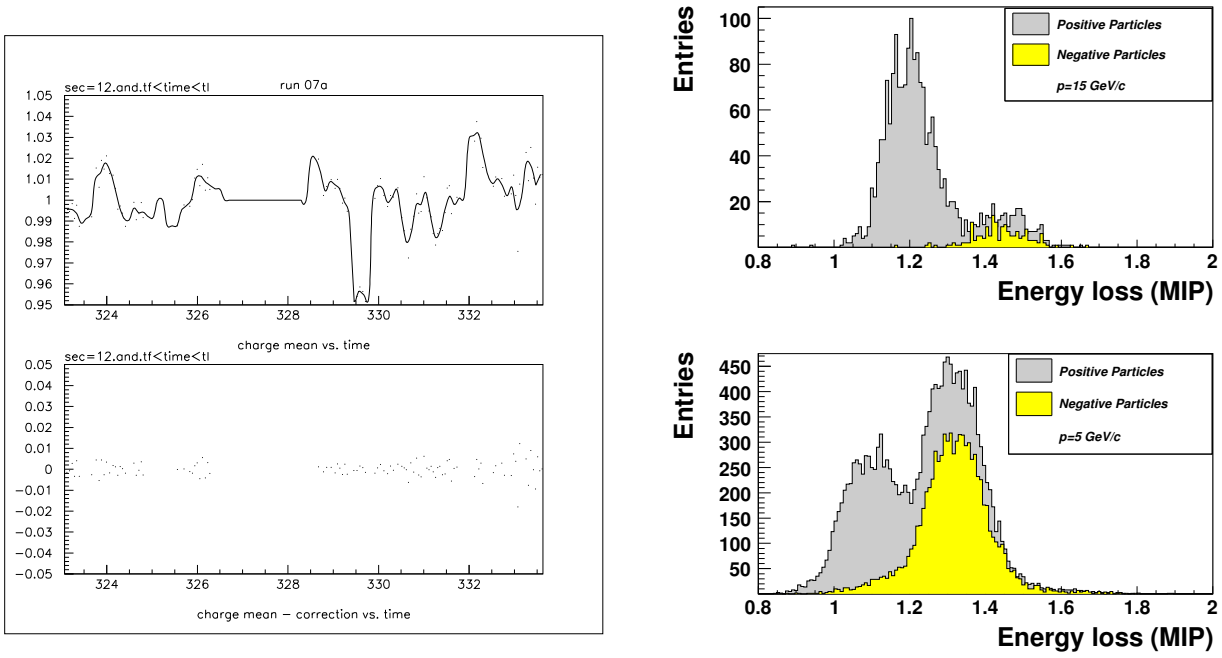

Figure 8: *Left:* Time dependence of the mean charge before and after correction. The line shown in the upper plot represents the correction function used. *Right:* Specific energy loss for positively and negatively charged particles at 5 and 15 GeV/c particle momenta.

6.4 Specific energy loss measurements

The optimization of the parameters required for the determination of the specific energy loss in the TPCs followed the method developed by NA49 and described in detail in Ref. [9]. Corrections for the following effects were calculated for the NA61 data:

- signal loss due to threshold cuts; the corresponding correction was obtained using Monte Carlo calculations performed for the gas mixture used in NA61;
- time dependence of the TPC gas pressure,
- residual time dependence,
- charge absorption during the drift,
- differences in the TPC sector gain factors,
- differences in the amplification of the preamplifiers and
- edge effects at sector boundaries.

Other corrections were taken from NA49 measurements because of limited statistics of the 2007 run. The correction for the residual time dependence is shown in Fig. 8 (left) as an example.

The corrected dE/dx spectra at 5 and 15 GeV/c are presented in Fig. 8 (right) and allow to estimate the resolution of the measurements to be about 4-5%.

6.5 Monitoring and QA software development

The NA61 off-line software predominantly consists of the software developed by the NA49 Collaboration. However, important NA49 packages for monitoring and quality assessment became obsolete and corresponding new software packages have been developed by NA61. In particular, this concerns software for:

- monitoring of the data reconstruction,
- off-line DST QA,
- event browsing.

These projects, as they are relevant for the data calibration and analysis, are briefly reviewed below.

6.5.1 Monitoring of the data reconstruction

In order to monitor the NA61 data reconstruction process running on the CERN batch farm, a dedicated software was developed. It allows fast browsing of the batch log files and provides quick access to the summary statistics such as number of processed events, of warnings and of errors in each individual output file of the production. It has web-oriented functionality and it is running with the help of a web-server. The main advantage of the selected scheme is the use of a simple HTML markup language and server scripts for parsing string information in the body of any log file requested by a user. The run file selection menu with corresponding report table and the possibility to access brief information on the execution of individual files are illustrated in Fig. 9. Fast access to the content of each individual log file is also possible via an HTML link.

6.5.2 Off-line DST QA

A dedicated software, called DST QA[1], is being developed for NA61 in order to assist in understanding the data quality of particular detectors and to help in the validation of the DST production.

The main steps of the DST QA are:

[1] QA stands for Quality Assessment or Quality Assurance.

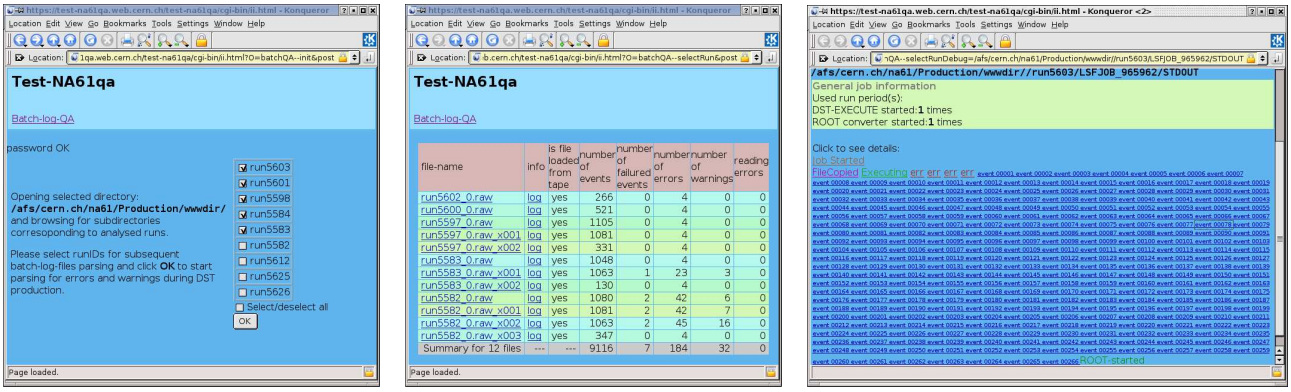

Figure 9: The selection menu for the log files to be analyzed for completeness of the batch processing is shown on the left browser window. In the middle window a general overview of the batch production status is seen for the selected files. One may go further into a brief overview of the file diagnostics during the DST production, as shown in the right window, to check individual events, warnings and errors as they appear in the log file with the help of HTML notations.

- preparation of a set of QA plots (histograms and scalers) for each detector and software module like e.g. tracking and particle identification,
- filling the QA control plots for each DST file during the production,
- fast visualization and semiautomatic monitoring of each QA plot as a function of time in order to detect files with unstable behavior of the detectors.

A dedicated QA-tool called `hhistory`[2] initially developed for the HADES experiment [11] was selected to perform fast browsing and semiautomatic scanning of the QA plots. It is realized as a stand-alone application under Linux, based on GUI classes from the ROOT library [10]. It allows:

1. fast histogram/file browsing with manual selection of status (quality) flags,
2. semi-automatic mean value scanning for the user-selected interval in one-dimensional histograms (see Fig. 10),
3. semi-automatic shape scanning for one-dimensional histograms [12],
4. semi-automatic absolute value scanning of one-dimensional histograms with the possibility to normalize the scanned histogram to the content of another histogram (per file).

[2]The abbreviation arises from histogram history.

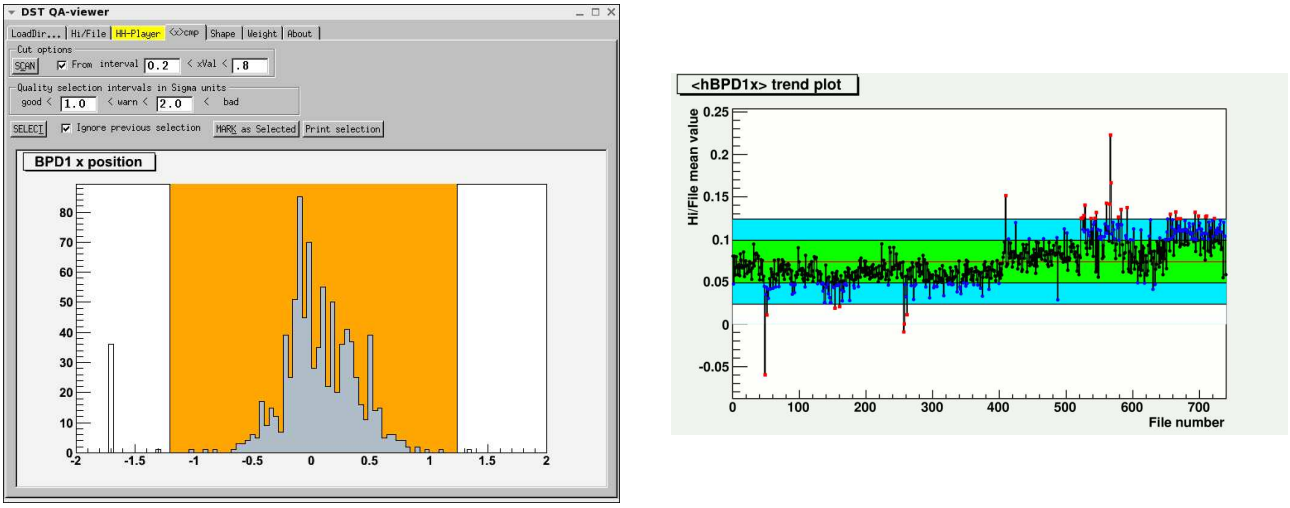

Figure 10: The `hhistory` selection menu for the mean value trend plot. The BPD1x distribution serves here as an example. In the left window it is shown how one selects an interval to be monitored for the mean value. In the right window the corresponding trend plot is presented. The whole procedure is completed within a few minutes.

Possibilities 2)-4) are equipped with an automatic selection for the file status/quality related to the analyzed histogram. A final decision on acceptance/rejection of the files for the subsequent DST analysis is left to the user's responsibility and can be based on the set of quality status results for pre-analyzed QA plots obtained with the `hhistory` tool.

The `hhistory` tool allows to create and store independent markup tables for different detector groups which later can be compared with each other in order to make a decision with respect to the file validation for the next iteration of DST production. This feature allows for distributed DST QA analysis. Alternatively it may indicate certain time intervals calling for better calibration of some detectors before the next iteration of DST production.

Integration of the off-line DST QA software with the monitoring of data reconstruction is under consideration. Furthermore, the package will be expanded in order to provide on-line raw data QA.

6.5.3 Event Display

A new event browser is under development to replace the various existing NA49 visualization tools by a single general purpose program that is easy to maintain. It is written in `C++` and uses the GUI capabilities of the `ROOT` [10] analysis framework. The current version can read and display the results of the event reconstruction either from the detailed `DSPACK` [13] or `ROOT` mini-DST files. For this purpose the event display can map each of the existing data structures to a new unified format based on `STL` [14] data containers. A screen shot of a typical thin target

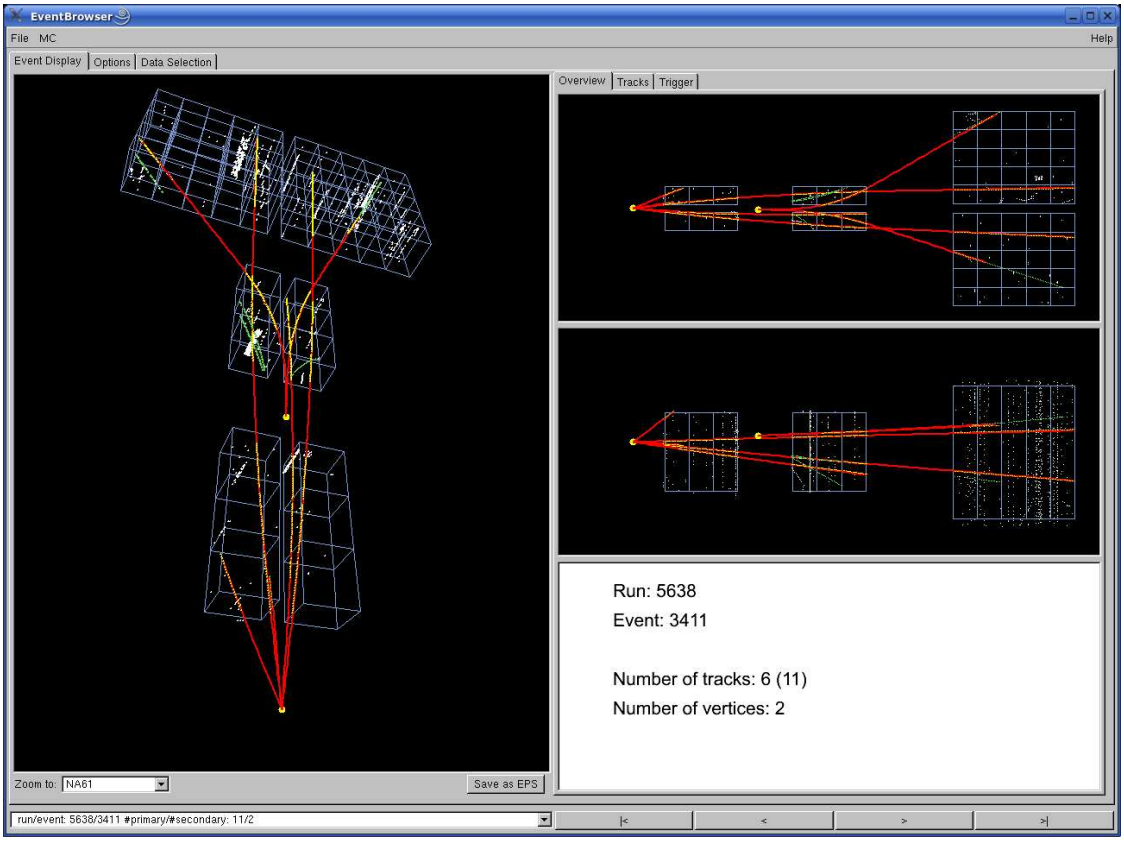

Figure 11: *EventBrowser* visualization of a 31 GeV/c proton on thin carbon target event. Reconstructed tracks and vertices are shown as red lines and large yellow circles respectively. TPC clusters that belong to the event are shown as yellow dots, hits belonging to unmatched tracks appear as green dots and noise hits are indicated by white dots. The left panel shows a three-dimensional view of the event, whereas on the right panel the top and side projections can be seen.

event visualized with the current beta-release of the *EventBrowser* is shown in Fig. 11.

7 Trigger and cross-section

7.1 Trigger and beam set-up

The NA61 experiment requires a minimum bias trigger to select interactions generated by a clean sample of protons of 31 GeV/c momentum. The layout of beam and trigger counters is presented in Fig. 12. The trajectory of incident beam particles is measured by 3 sets of proportional chambers, the Beam Position Detectors. Beam particles are identified by two Cerenkov

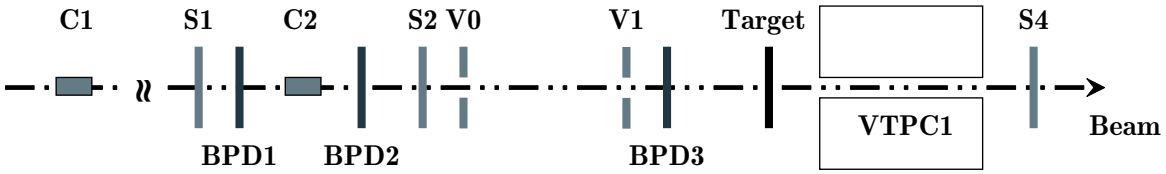

Figure 12: The layout of the NA61/SHINE beam and trigger counters.

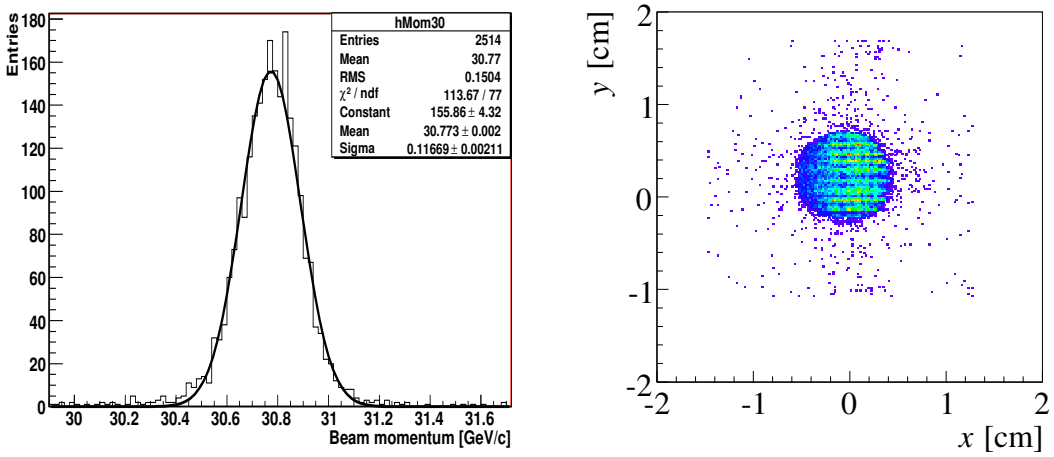

Figure 13: *Left:* The distribution of the proton beam momentum measured by the NA61/SHINE TPCs in a special run during the 2007 data taking. *Right:* The beam spot as measured by BPD-3.

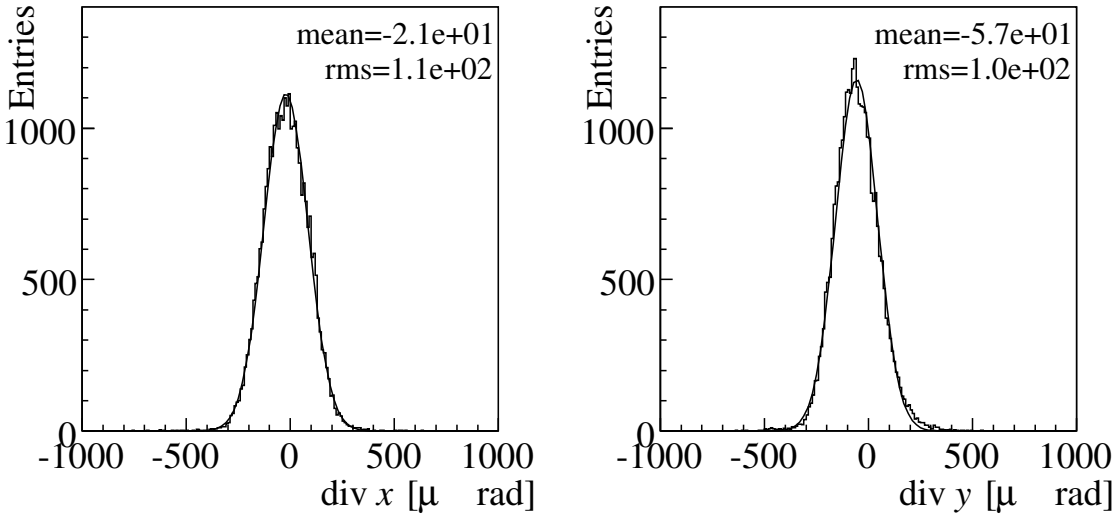

Figure 14: The beam divergence in x (left) and y (right).

counters, a CEDAR and a threshold counter, labeled C1 and C2, respectively. The CEDAR counter, through the use of a 6-fold coincidence, provides positive identification of protons, while the threshold Cerenkov counter, operated at a pressure lower than the proton threshold, is used in anti-coincidence in the trigger logic. Two trigger counters S1 and S2, together with two veto counters V0 and V1, with a 1 cm diameter hole to define the acceptance region of the beam, complete the beam trigger setup. Beam protons are selected by the coincidence $=\text{S1}\cdot\text{S2}\cdot\overline{\text{V}}\cdot\text{C1}\cdot\overline{\text{C2}}$, with V representing the OR of the two veto counters. Measured beam momentum, beam profile and divergences are shown in Figs. 13 and 14. Scans of the CEDAR and threshold Cerenkov counters measured a proton percentage of 15% in the beam.

The use of a thin target of only 4% of an interaction length requires the use of an interaction trigger. Interactions are selected by anti-coincidence of the incoming beam particles with a small, 2 cm diameter, scintillation counter (S4) placed in the beam line between the two vertex magnets. This interaction trigger is a minimum bias trigger based on the disappearance of the incident proton particle. A preliminary measurement of the total inelastic cross section based on the data collected with the thin target is discussed in subsection 7.2.

Given the large absorption probability of the T2K replica target, there is no need of a dedicated interaction trigger, therefore all beam triggers were recorded. For the 2008 run we foresee to add an additional trigger counter, with the same cross section as the diameter of the T2K target, mounted just upstream of the target. This will insure that the selected beam particles will go through the target, increasing our trigger efficiency.

The transverse positions of the incoming beam particles are measured by three beam position

detectors (BPD-1/2/3) along the beam line. For the 2008 run the old BPD counters will be replaced by the new ones. The active area of the new detectors was increased by a factor of 2.25 with respect to the old ones and is 48×48 mm^2. Two orthogonal sense wire planes (15 μm tungsten wires with 1.5 mm pitch) are located between three cathode planes made of 25 μm aluminized Mylar. The cathode readout planes are sliced into 32 strips of 1.5 mm pitch which are connected to the readout electronics. The chambers are operated with an $Ar : CO_2$ (90:10) gas mixture.

7.2 Inelastic Cross Section

A preliminary analysis of the 2007 run data with the thin target configuration results in an interaction probability of $(7.07 \pm 0.01)\%$ for inserted target operation and of $(1.76 \pm 0.01)\%$ for empty target operation. These measurements lead to an interaction probability of $(5.35 \pm 0.01)\%$ due to the thin target, resulting in a 'trigger' cross section of (297.5 ± 0.7) mb, after correcting for the exponential beam attenuation in the target. The total inelastic cross section σ_{inel} can be derived from the 'trigger' cross section by applying three major corrections:

- Subtract the σ_{elastic} contribution,
  i.e. remove those events where the primary particle undergoes a large angle coherent elastic scattering on the target nuclei and does not reach S4. Therefore a trigger on the event is present even if no proton interaction occurred.

- Add the $\sigma_{\text{loss}-\text{p}}$ contribution,
  i.e. take into account interactions where a secondary proton hits S4 and therefore prevents from triggering on the event. The major contribution comes from incoherent elastic scattering of the incident protons on the individual nucleons of the nuclei (quasi-elastic scattering).

- Add the $\sigma_{\text{loss}-\pi/\text{K}}$ contribution,
  i.e. take into account interactions where a secondary pion or kaon at high x_F hits S4 and therefore prevents from triggering on the event.

These corrections have been estimated up to now relying on the GEANT4 [15] simulation of the trigger setup, using the measured profile and divergence for the incoming proton beam.

Angular distributions for coherent elastic scattering and quasi elastic scattering (see Fig. 15) as well as total cross section values in GEANT4 have been cross-checked against available experimental measurements[3], as shown in Table 1.

We found good agreement between the GEANT4 simulation and the known experimental values, however we note a 12% discrepancy on the total elastic cross section value.

[3]Note that although the energy dependence is rather flat, the literature values have been obtained at different proton momentum.

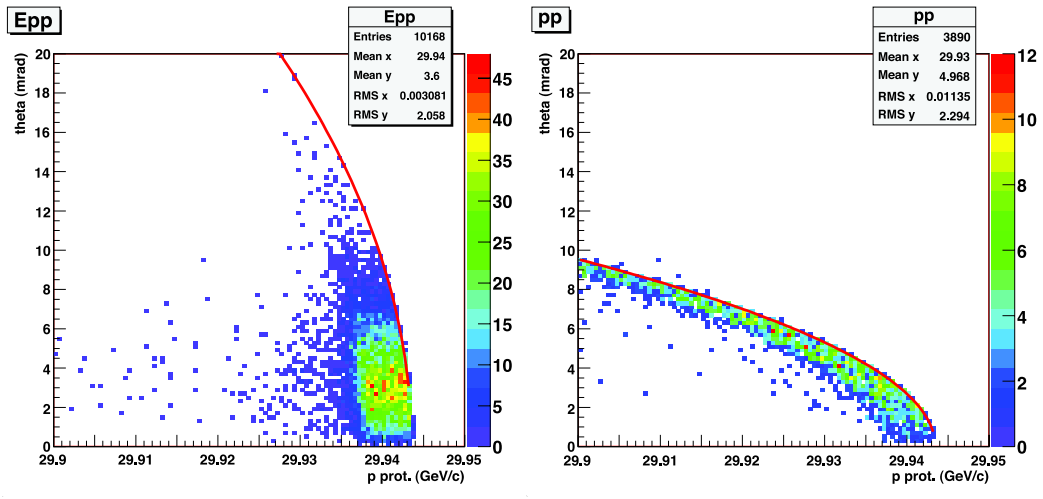

Figure 15: *Left:* Angular distribution of protons undergoing coherent elastic scattering on the nucleus. *Right:* Angular distribution of protons undergoing quasi-elastic scattering on individual nucleons (from simulations using GEANT4).

σ **contribution**	**expected (mb)**	**GEANT4 (mb)**
σ_{inel} tot.	254 [16], 247 [17], 251 [18]	244
$\sigma_{elastic}$ tot.	81 [16]	72
$\sigma_{elastic}$ out of S4	54 [16] (67%)	49.5 (69%)
$\sigma_{quasi-elastic}$ tot.	29 [16]+[19]	27
$\sigma_{quasi-elastic}$ out of S4	27 [16]+[19] (93%)	24 (89%)

Table 1: Comparison between GEANT4 simulation and expected values from previous experiments. The percentage indicates the fraction of protons missing S4.

σ **contribution**	**value (mb)**
$\sigma_{trigger}$	297.5 $\pm$0.7
σ_{loss-p}	5.8 $\pm$0.2
$\sigma_{loss-\pi/K}$	0.6 $\pm$0.06
$\sigma_{elastic}$ contribution	-49.2 $\pm$0.6
σ_{inel}	254.7 $\pm$1.0

Table 2: Cross section corrections estimated using GEANT4 simulation. Note that the errors are only statistical.

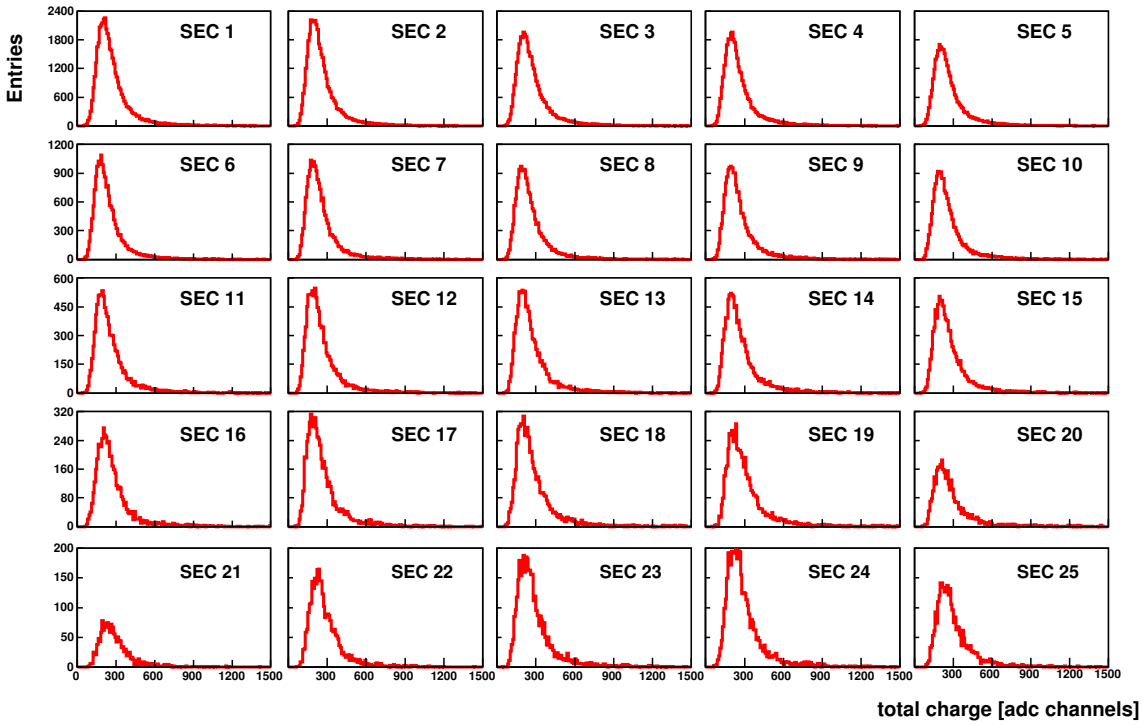

Figure 16: Typical distributions of the total charge collected in reconstructed clusters in each MTPC-R sector for the 2007 run.

The corrections to the 'trigger' cross section, summarized in Table 2, result in a total inelastic cross section of $\sigma_{inel} = 254.7 \pm 1.0$ mb, where the quoted error is only statistical.

This preliminary value for the inelastic cross section is in good agreement with previous measurements. We note that if we increase by 12% the total elastic cross section in GEANT4, as suggested by the data in [16], we would get a total inelastic cross section of 249 mb. The next steps will be to get a better estimate of $\sigma_{\mathrm{loss-p/\pi/K}}$ and $\sigma_{\mathrm{elastic}}$ from the data themselves and to perform an evaluation of the systematic errors.

8 Detector performance and raw spectra

In this section the NA61 performance for the measurement of identified hadron production will be discussed and uncorrected spectra of identified hadrons will be presented. The results are mainly for the p+C data taken with the thin target at 31 GeV/c, unless otherwise stated.

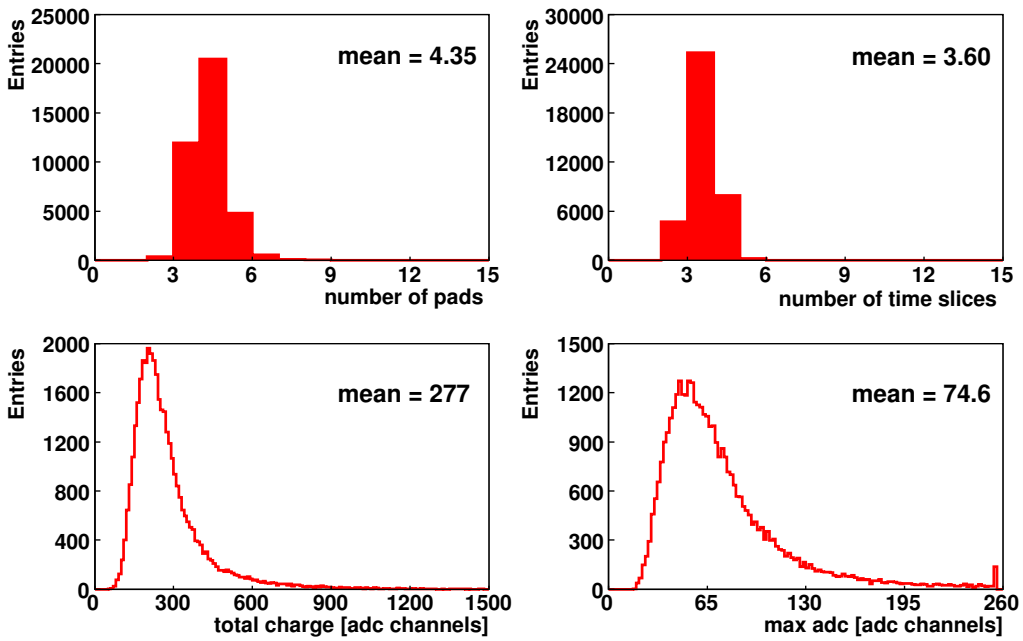

Figure 17: Typical distributions of cluster parameters in the sector 3 of the MTPC-R: the number of pads (upper left), the number of time slices (upper right), the total charge (bottom left) and max-adc (bottom right).

8.1 Tracking performance

A rather complicated clustering and tracking algorithm developed for the NA49 experiment and inherited by NA61 starts from the recognition of clusters found in the TPC detectors. These clusters of connected areas in the pad-time planes which result from the primary ionization left along the trajectories of charged particles. All sectors of vertex (VTPC-1, VTPC-2) and main (MTPC-L, MTPC-R) TPCs were fully operational during the 2007 run and thus contain cluster data. Typical distributions of the total charge of clusters for all sectors of the MTPC-R are shown in Fig. 16. The total charge as well as other cluster properties like number of pads, number of time slices and maximum adc value in the cluster, are similar (see Fig. 17) to those obtained in NA49. The center-of-gravity of clusters, the TPC points, found in the first step of the data reconstruction process is used in the tracking algorithm. First, this algorithm builds track fragments in each TPC detector separately. Such track fragments are then extrapolated to other detectors and matched to their counterparts. Reconstructed global tracks are used for the momentum fit employing the Levenberg-Marquardt method [20]. The fit minimizes the χ^2 based on the deviations (residuals) of the measured points from the fitted trajectory. Fig. 18 (left) shows a distribution of the number of points included in global tracks. The structure of the TPCs with different number of pad-rows and sectors (VTPC-1, VTPC-2 = 72 (3×24)

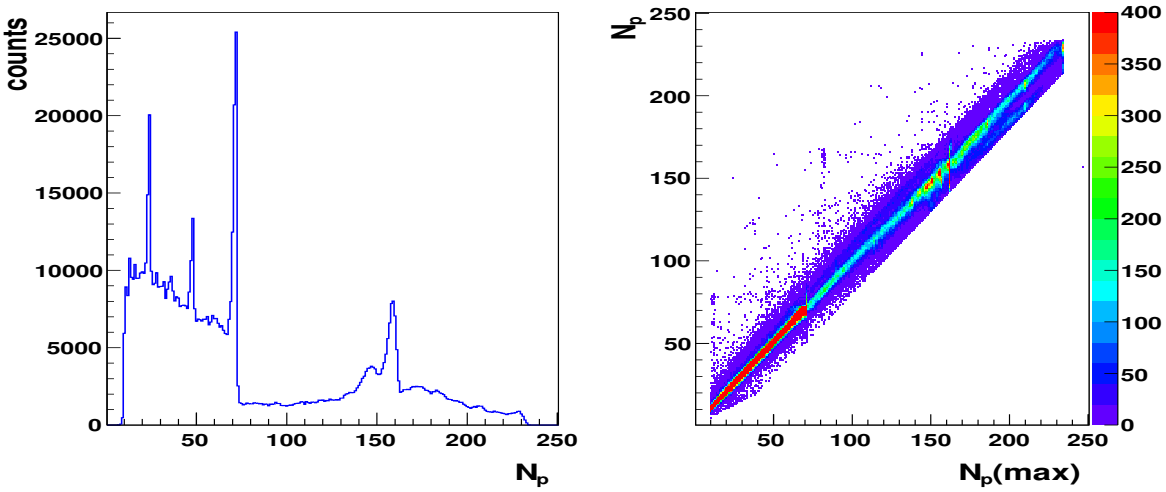

Figure 18: The distribution of the number of points (left) and the number of points versus maximal number of points (right) for reconstructed global tracks.

and MTPC-L/R=90 (5×18)) is clearly visible. A distribution of the number of points N_p as a function of the maximal number of points $N_p(max)$ calculated from the track trajectory is presented in Fig. 18 (right). The N_p for the most of tracks is close to the $N_p(max)$ indicating a high efficiency of the TPCs and of the clustering and tracking algorithms.

The statistical uncertainty of the TPC points used for the calculation of χ^2 is estimated from the width of the residual distribution of the point positions around the tracks in x and y coordinates, separately. Examples of such distributions are shown in Fig. 19.

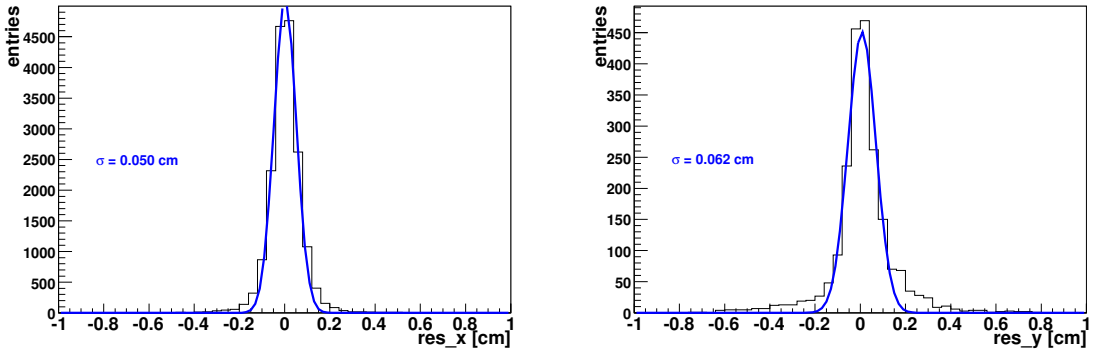

Figure 19: Example of residual distributions in VTPC-1 for x and y coordinates. The non-Gaussian tails are cut in order to estimate the width of the Gaussian peak.

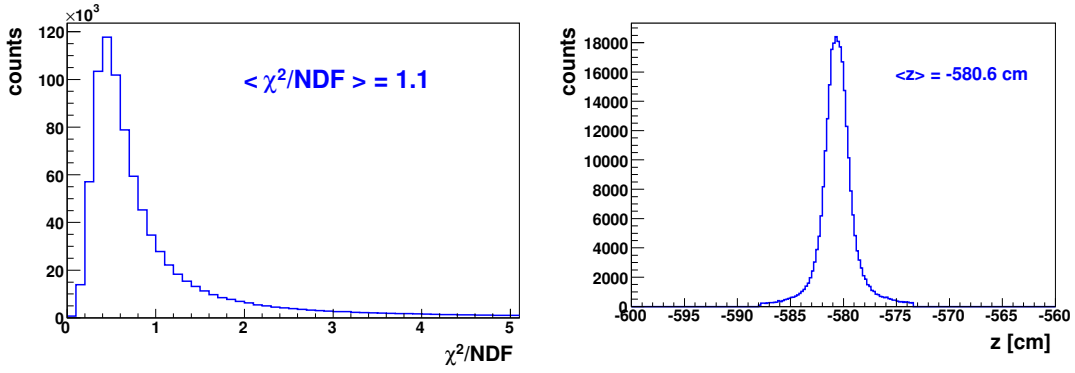

Figure 20: *Left:* Distribution of χ^2/NDF of the momentum fits for reconstructed global tracks. *Right:* The z-position of the reconstructed primary vertex for the thin target runs.

The statistical uncertainty of the point position used by the track fit algorithm is parametrized by a function depending on the drift length, the angle of the track, the number of pads within the cluster and the region of the TPC. Since the gas mixture in the TPCs in NA61 differs from the one used in NA49, a new parametrization of the uncertainties is needed. However, due to the limited statistics of the 2007 data this new parameterization could not be derived. Therefore, the NA49 parameterization of the statistical errors is currently used. Fig. 20 (left) shows the distribution of χ^2/NDF of momentum fits for the reconstructed global tracks. The mean value is close to 1, indicating that the NA49 parametrization is approximately valid also for the NA61 data.

The NA61 reconstruction software initially calculates the track momentum at the first measured point and later, after reconstruction of the primary interaction point (see description below), also the track momentum at the primary interaction. The statistical resolution of the momentum determination was determined for the beam tracks measured in the VTPC-2 and MTPC-L detectors (see Fig. 13, left) and it is consistent with the one estimated by NA49.

Global tracks with momenta determined at the first measured TPC point are tracked in the magnetic field upstream and used to fit the position of the primary interaction. In the fit procedure the primary interaction point is assumed to be located on the beam particle trajectory measured by the BPD detectors. Thus, only the z-coordinate of the interaction point is fitted. The distribution of the z-coordinate of the primary interaction for the thin target runs is shown in Fig. 20 (right). A narrow peak is observed around the nominal target position. The consistency and the resolution of the procedure is demonstrated in Fig. 21, where the track impact parameter distributions are shown. Here, the track impact parameter is defined as the distance between the interaction point and the back extrapolated track in the target plane. The distributions of the x and y components of the track impact parameter are centered at zero and have a width of about 0.5 cm.

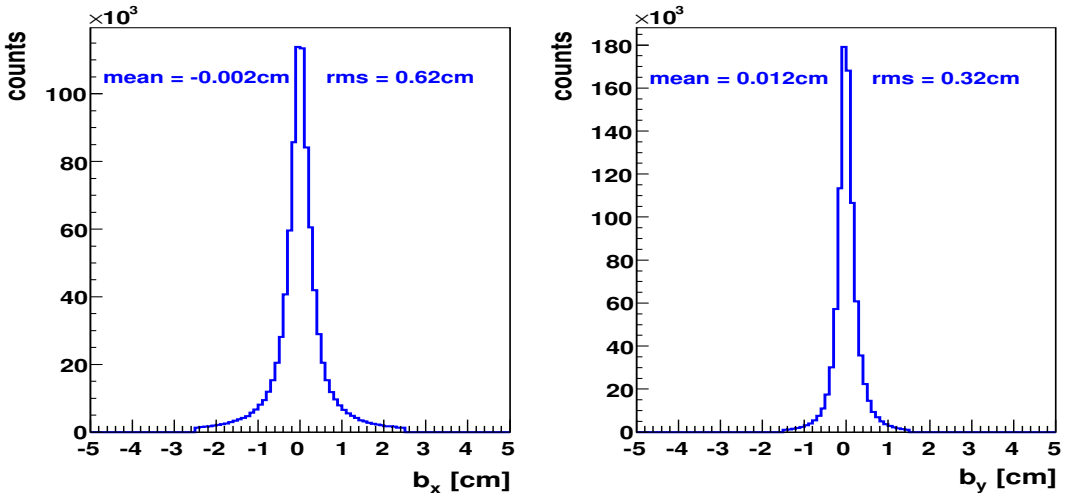

Figure 21: The distributions of the x (left) and y (right) components of the track impact parameter.

8.1.1 Runs with the T2K replica target

The runs taken with the T2K replica target have also been reconstructed. The corresponding data are currently being analyzed. As an example we show here the distribution of the z-position of the reconstructed primary vertex for the replica target runs in Fig. 22.

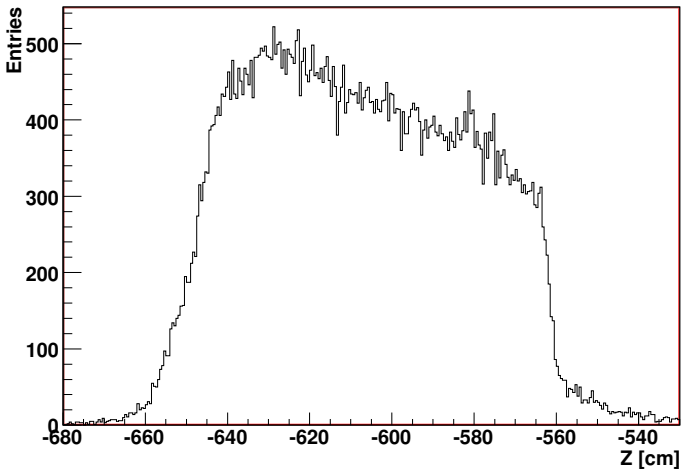

Figure 22: The z-position of the reconstructed primary vertex for the T2K replica target runs.

8.2 Event selection

Suitable off-line event selection is necessary in order to clean up the event sample and reduce the background coming from non-target interactions. A preliminary list of event cuts for the thin target data together with their impact on the event sample is presented in Table 3. The first event cut listed requires that the incident beam particle was measured in each BPD and therefore ensures that the beam track is well defined. The second quantity that is considered is a flag that has been set in each event during the reconstruction. If the fit to determine the z-position of the main vertex converges after some iterations, the `vertex.iflag` is set to 0. In case the fit diverges or other problems occur during the reconstruction, it is set to non-zero values. Only events with `vertex.iflag=0` are currently analyzed. To select interactions in the target region only, it is furthermore required that the fitted z-vertex position is close to the nominal one. The results presented below are obtained using the described event selection procedure.

Cut	**Effect**
Cut on the BPD Position	77.8%
`vertex.iflag = 0`	60.1%
Cut on the z-Vertex Position	41.3%

Table 3: The event cuts and the fraction of events passing them if applied one after another.

8.3 Negatively charged hadrons

The analysis of negatively charged hadrons from the primary interaction, further referred to as h^- analysis, is based on estimates that more than 90% of produced negatively charged particles at the SPS energies are π^- mesons. The remaining small fraction includes K^- mesons and electrons from π^0 Dalitz decays and a negligible number of anti-protons. If we neglect this admixture, preliminary information on the differential cross sections for π^- production from p+C interactions at 31 GeV/c can be obtained even before detailed PID studies. This is not the case for positively charged particles due to the large fraction of protons and K^+ mesons in the final state.

The h^- analysis starts from the selection of negatively charged particles from the primary vertex. Then a Monte-Carlo simulation is used to calculate corrections for the geometrical acceptance, the reconstruction efficiency, and the non-pion admixture. Finally, the corrected spectra of π^- mesons are obtained. These spectra will be compared with the corresponding results obtained using particle identification by dE/dx and tof measurements. This comparison should lead to a reliable estimate of systematic errors of the final results.

The preliminary results presented here are based on an analysis of all thin target runs collected during the 2007 run. The analyzed runs contained 671607 events. Event quality cuts

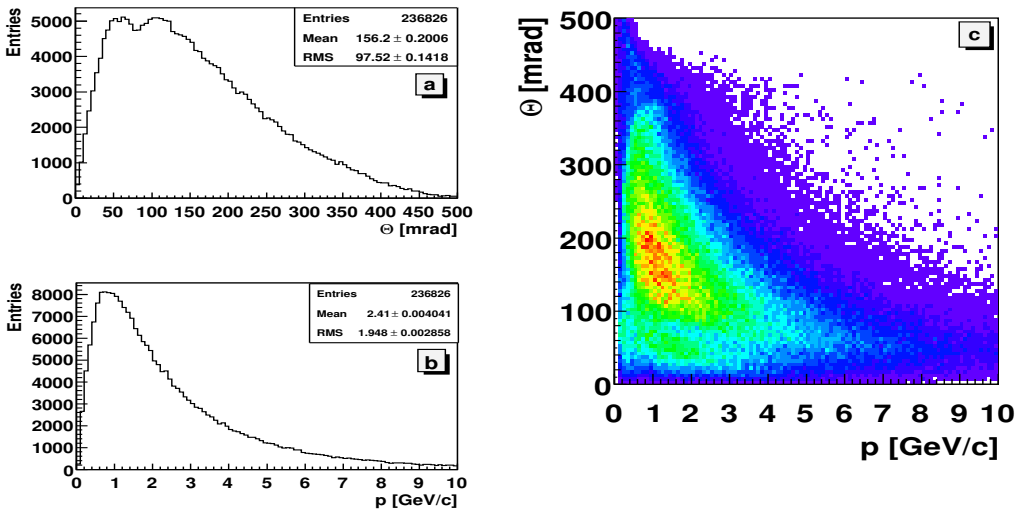

Figure 23: The uncorrected spectra of negatively charged particles in p+C interactions at 31 GeV/c registered by NA61: the distributions of polar angle (a), momentum (b) and the (polar angle – momentum) plane (c).

following the description presented in subsection 8.2 were applied.

In 277 k selected events, there were about 1 M tracks, corresponding to approximately 4 tracks per event on average. Among those tracks, 662 k were positively charged (63% of all tracks) and 382 k were negatively charged (37% of all tracks). Only negatively charged tracks entered further analysis. Additional cuts on the quality of the individual reconstructed track were applied. The effects of the quality cuts on the number of negatively charged tracks are summarized in Table 4.

Table 4: The effect of track quality cuts for the negatively charged track sample.

All negative tracks	382046 (100%)
Independent Momentum determination: Minimum number of points found in VTPC1+2 is 5	373163 (98%)
Cut on the ratio of measured and potential points: Ratio larger than 0.5	372772 (97%)
Cut on the impact parameter	326053 (85%)
Cut on the number of potential points (larger than 30)	236826 (62%)

The distributions of the number of selected negatively charged particles in (polar angle – momentum) and (transverses momentum – rapidity) planes, as well as their projections are

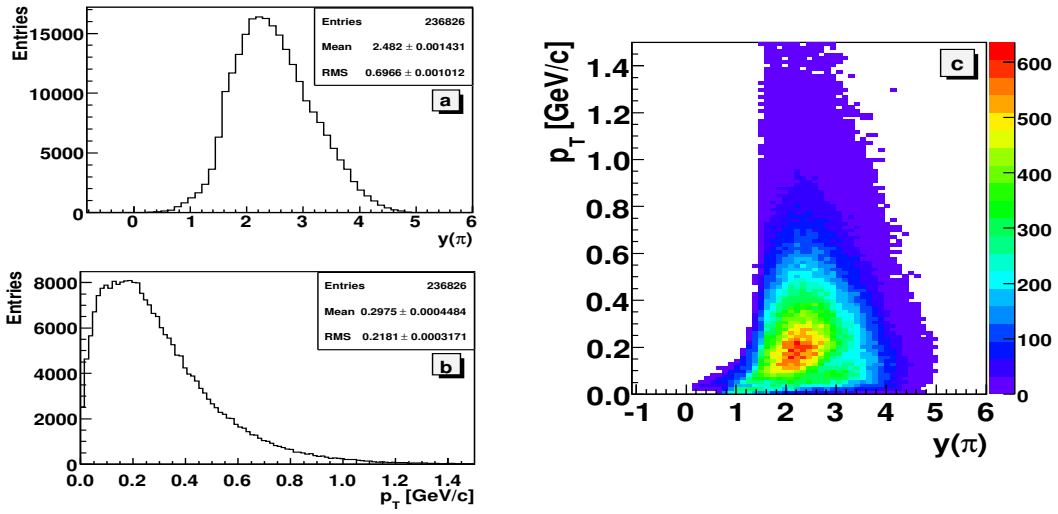

Figure 24: The uncorrected spectra of negatively charged particles in p+C interactions at 31 GeV/c registered by NA61: the distribution of rapidity calculated in the lab. system assuming pion mass (a), transverse momentum (b) and the (transverse momentum – rapidity) plane (c).

shown in Figs. 23 and 24. The spectra are not corrected for acceptance and reconstruction efficiency. It is seen that the phase space needed for the T2K measurements is covered by the NA61 data. Almost the complete domain above mid-rapidity ($y(\pi) = 2.08$ for p+p interactions) is detected, whereas there is only a limited coverage for $y(\pi) < 1.5$.

Simulations performed using the VENUS model show that about 30% of all charged hadrons produced in p+C interactions at 31 GeV/c are in the NA61 TPC acceptance.

8.4 Particle identification by decay topology measurements

The search for and the reconstruction of track topologies resulting from the weak decays of hadrons are included in the NA61 reconstruction chain. Strategies and software packages inherited from the NA49 reconstruction chain are used. They include the search for and the reconstruction of:

- the "V^0"-topologies which allow to identify decays of Λ and $\overline{\Lambda}$ hyperons and K^0_S mesons,
- the "cascade"-topologies which allow to identify decays of multi-strange hyperons and anti-hyperons (Ξ, $\overline{\Xi}$, Ω, $\overline{\Omega}$) and
- the "kink"-topologies which allow to identify decays of charged kaons.

The main steps are illustrated using as an example the "V^0" search, reconstruction and identification. In this case one looks for charged decays of neutral hadrons: $\Lambda \rightarrow \pi^- + p$, $\overline{\Lambda} \rightarrow \pi^+ + \overline{p}$ and $K^0_S \rightarrow \pi^- + \pi^+$.

First, pairs are formed of all positively charged with all negatively charged particles. The tracks were reconstructed by a global tracking algorithm that connects the track parts registered in the different TPCs. The momentum of each track was fitted at the first measured point of this track and is used to track back the particle trajectory from this point towards the target plane. The pair is identified as a V^0 candidate if the distance of closest approach between the trajectories of the two particles is less than 0.5 cm.

Second, the best estimate of the position of the decay point as well as of the momenta of the decay products at this point is obtained by a χ^2 minimization procedure. The results are stored in the DST.

Third, the decay kinematics, different for different decay hypotheses, allows a (statistical) identification of the reconstructed V^0s. This is done either by the analysis of the invariant mass spectra calculated for different decay hypothesis or by performing a kinematic fit.

A significant number of Λ and K^0_S can be identified in the 2007 data. This is illustrated in Fig. 25, where the distribution of the V^0 candidates reconstructed in p+C interactions at 31 GeV/c is plotted in the Podolanski-Armenteros variables [21]. The invariant mass distribu-

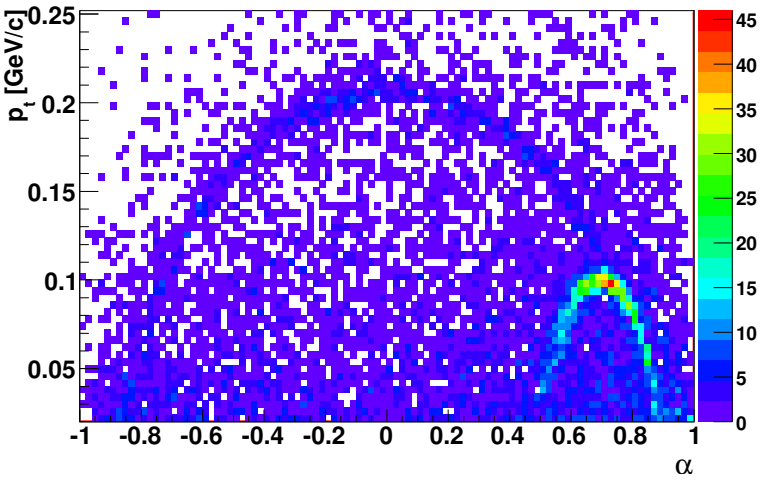

Figure 25: Spectrum of all V^0 candidates reconstructed in p+C interactions at 31 GeV/c in the Podolanski-Armenteros variables [21]. The K^0_S and Λ signals are clearly visible.

tion plotted under the Λ decay hypotheses is shown in Fig. 26. Here, only V^0 candidates with a distance between the fitted V^0 vertex and the interaction vertex larger than 10 cm are plotted. This selection leads to a significant reduction of the background entries and preserves a large fraction of the signal. The FWHM of the signal distribution is about 6 MeV which is similar to the corresponding resolution measured by NA49 [22].

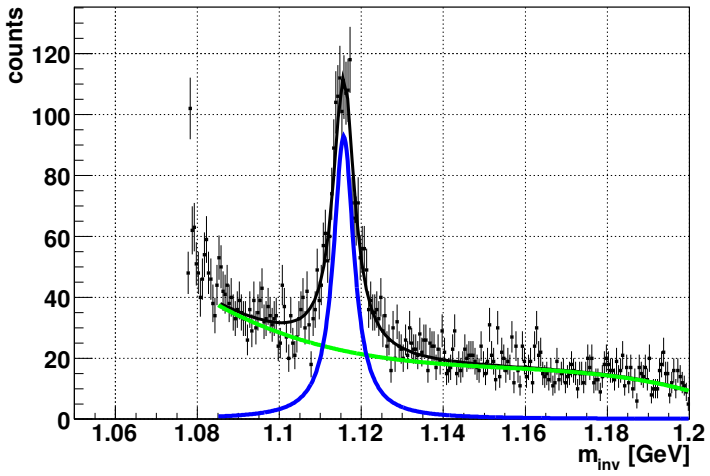

Figure 26: Invariant mass distribution of the selected V^0 candidates in p+C interactions at 31 GeV/c obtained for the Λ decay hypothesis. The background has been parametrized by a fourth order polynomial, and the signal by a Lorentzian distribution.

The maximum kinematic acceptance of the 2007 data is presented in Fig. 27, where selected V^0 candidates are plotted in the $p - \theta$ and $y - p_T$ planes.

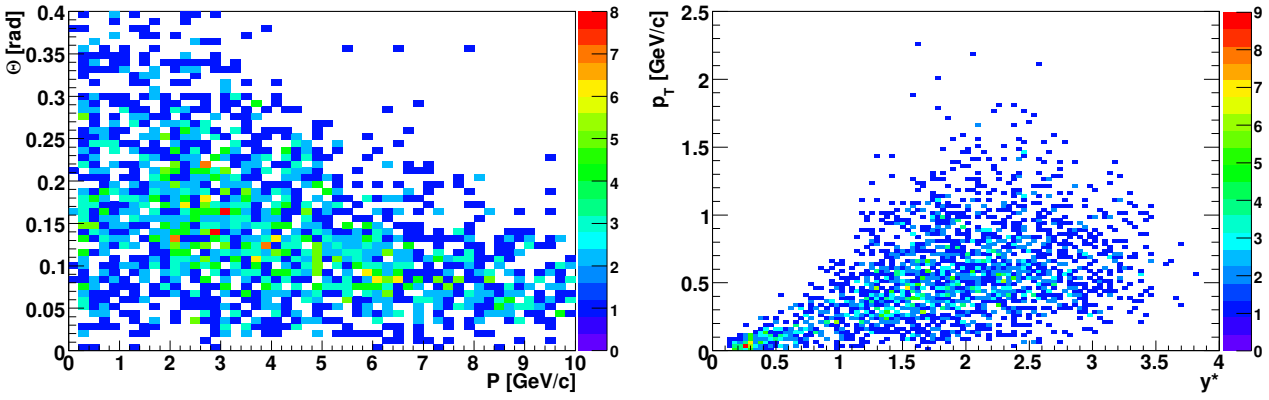

Figure 27: The spectra of selected V^0 candidates in $p - \theta$ (left) and $y^* - p_T$ (right) planes.

8.5 Particle identification by dE/dx measurements

Particle identification algorithms using the specific energy loss in the TPCs developed by the NA49 collaboration [9] are now being used for the NA61 experiment.

The NA61 TPCs do not measure the energy loss of the particle but rather the energy deposited by the ionization processes in its active volume. When carrying out PID by specific ionization measurements, one assumes that these quantities are directly proportional. The amount of the produced ionization is measured by the total number of electrons collected per unit length of track in the TPCs. There are two components contributing to the total yield of electrons: primary and secondary ionization. The ionization produced directly by the incident track is referred to as primary. If liberated electrons have an energy E above the value required to produce an ion pair, further (secondary) ionization, can be produced.
The energy loss distribution per unit track length is described by the Landau distribution. The mean value and width of the distribution of energy loss samples on the track is sensitive to the large energy fluctuation in the ionization process. Therefore a truncated mean technique is used for quantifying the mean $\frac{dE}{dx}$. In this method, the highest and lowest measurements are rejected for each track. For all data collected during the 2007 run the (0:50) truncation was applied, which means that only 50% of clusters with the lowest energy deposition are kept for the determination of the mean $\frac{dE}{dx}$.

Scatter plots of the energy loss, i.e. the truncated mean $\frac{dE}{dx}$ value of the track (in MIP units[4]), versus the particle momentum in the laboratory frame is shown in Fig. 28 for positively and negatively charged particles produced in p+C interactions at 31 GeV/c. For positively charged hadrons clear bands corresponding to pions and protons are seen, whereas for negatively charged hadrons the pion band dominates.

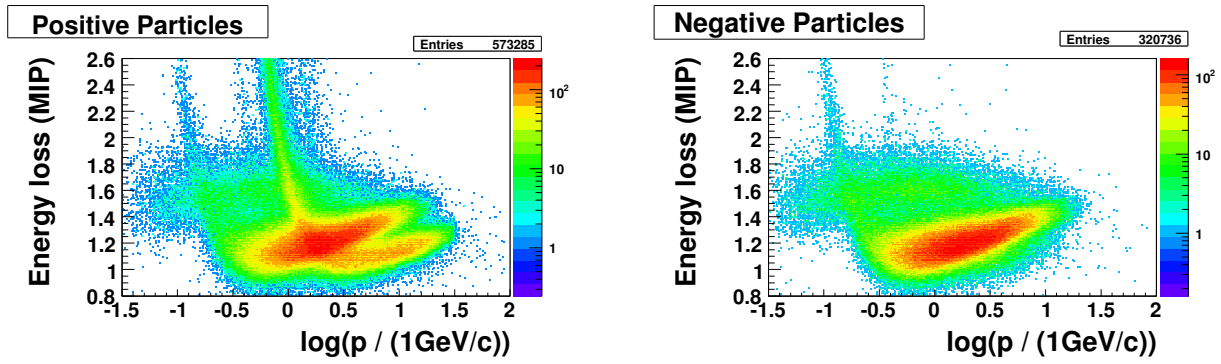

Figure 28: Truncated mean $\frac{dE}{dx}$ as a function of momentum for p+C interactions at 31 GeV/c beam momentum for positively and negatively charged particles, respectively. Note the logarithmic scale.

When the truncated mean $\frac{dE}{dx}$ spectra are plotted in narrow momentum bins the distributions of different particle species are centered at different values of $\frac{dE}{dx}$ (e.g. see Fig. 8, right). This in turn allows a determination of identified hadron yields.

[4]MIP unit - the amount of the ionization caused by a Minimum Ionizing Particle.

For determination of particle yields several steps should be performed:

1. *Selection of a specific region (bin) of phase space*
   In the relativistic rise region, the Bethe-Bloch functions increase with momentum, therefore the width of the bin should be small enough to avoid smearing of the spectrum. In the preliminary analysis bins of θ and total momentum were chosen.

2. $\frac{dE}{dx}$ *Fit Function*
   The 50% truncation transforms the Landau distribution of the samples into a Gaussian distribution of the mean per track if the number of samples stays above about 30 (see Ref. [9] for more details). The experimental $\frac{dE}{dx}$ histograms will be fitted by a sum of Gaussian distributions corresponding to all relevant particle species: (anti)protons, electron/positrons, pions and kaons.

3. *The Fit Parameters*
   The fit has nine parameters: four particle yields, four mean $\frac{dE}{dx}$ values and the σ parameter describing the width of the individual distributions. In principle the last five parameters should be known exactly from the energy loss function and the resolution function if these quantities could be absolutely predicted. Due to the complexity of the primary and secondary ionization processes this prediction is not possible at the level of precision needed here.

4. *Fit Procedure*
   Optimization of the parameters is performed by using the maximum log-likelihood method. The quality of the fit is checked by comparison of the fitted functions to the experimental $\frac{dE}{dx}$ histograms.

Following the above steps one will obtain raw particle yields which still need to be corrected for:

- geometrical acceptance,
- reconstruction efficiency,
- particle decays,
- feed down contamination, i.e. the contribution of secondary particles which are decay daughters of other particles and accidentally reconstructed as primary ones.

The first estimate of the NA61 dE/dx resolution shows that it is similar to that achieved by NA49 (4-5%). Thus, as in NA49, particle identification in the momentum range 4-50 GeV/c should be possible from the dE/dx measurements alone.

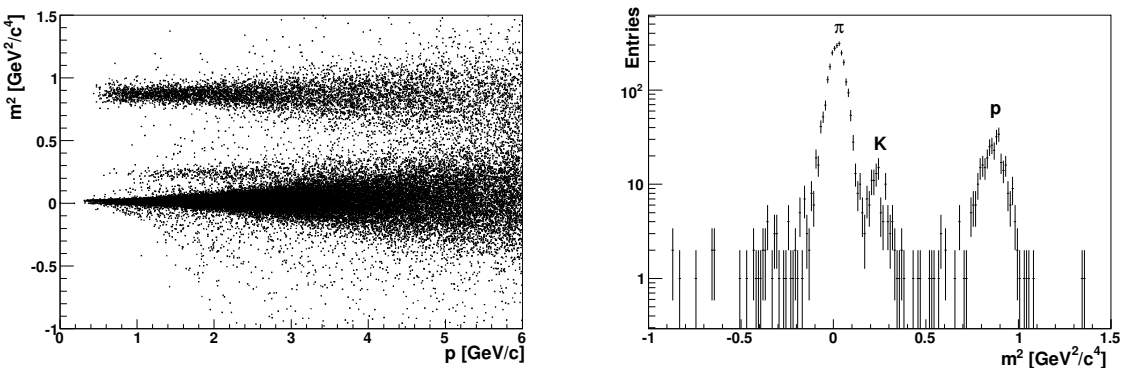

Figure 29: Preliminary results for the PID performance of the ToF-F detector. *Left:* Mass squared versus momentum. *Right:* Mass squared for the momentum range $1 < p < 3$ GeV/c. Accumulations corresponding to pions, kaons and protons are clearly visible.

8.6 Particle identification by tof measurements

Particle identification by the time-of-flight method is based on the relation between the particle mass, momentum and velocity:

$$m = p\sqrt{\frac{c^2t^2}{L^2} - 1}\ .$$

In the NA61 experiment the TPCs allow precise measurement of the track length L and of the particle momentum p. The time t is precisely measured by the 3 ToF walls: ToF left and right (ToF-L, ToF-R) and forward ToF (ToF-F). After preliminary calibration, the calculated resolution is 100 ps for both ToF-L/R and better than 130 ps for the ToF-F. Fig. 29 shows a plot of the mass squared versus momentum and a histogram of mass squared in a selected momentum range of 1-3 GeV/c in ToF-F for all thin target runs. Pions, protons and kaons are clearly visible. Pions can be separated from protons up to about 8 GeV/c momenta, while kaons are visible in the 1-3 GeV/c range. A 130 ps time resolution should yield a 2.5 σ π/K separation at 4 GeV/c. By improving the geometrical calibration and/or by refining the t_0 calculation we are confident that the goal of π/K separation at 4 GeV/c can be reached.

The particle identification with the help of the ToF-L/R system is illustrated in Fig. 30. Here, the squared mass calculated using tracking (momentum p and track length L) and time-of-flight (ToF-L/R) measurements is plotted as a function of the particle momentum. The kaons are separated from the pions in the momentum region of $p < 3.5$ GeV/c; the protons are well isolated in m^2 in the whole range studied up to $p = 6$ GeV/c.

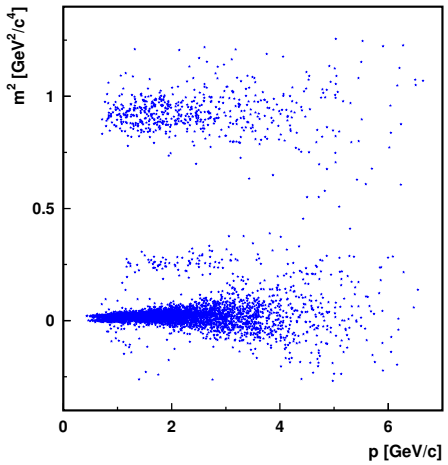

Figure 30: Mass-squared from ToF-L/R versus momentum in 2007 p+C data.

8.7 Particle identification by combined dE/dx and *tof* measurements

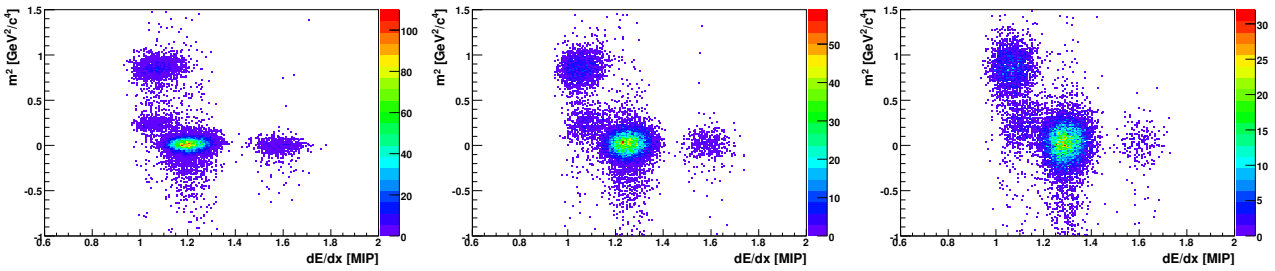

Figure 31: Examples of combined ToF and dE/dx PID performance for positively charged particles in the momentum range 2-3 GeV/c (left), 3-4 GeV/c (middle) and 4-5 GeV/c (right). Four clear accumulations corresponding to positrons, pions, kaons and protons are observed.

For particles in the acceptance of the ToF detectors dE/dx information from the TPCs is available simultaneously with the time of flight. This is demonstrated in Fig. 31, where particles in various momentum ranges are sorted corresponding to their dE/dx signal and the mass squared obtained from the forward time-of-flight and momentum measurement.

At momenta above approximately 4 GeV/c the separation of the lighter particles (e, π) from the group of heavier ones (K, p) is performed essentially by dE/dx, whereas the ToF

measurement is needed to distinguish between kaons and protons. Below 4 GeV/c particle identification can be performed almost exclusively by the ToF.

Even though the dE/dx is momentum dependent a preliminary selection is possible in the whole momentum range 0-6 GeV/c. Fig. 32 presents the $p - \theta$ plot for negative and positive pions and kaons selected with this method. The whole region of interest for the T2K studies is covered (compare with Fig. 2).

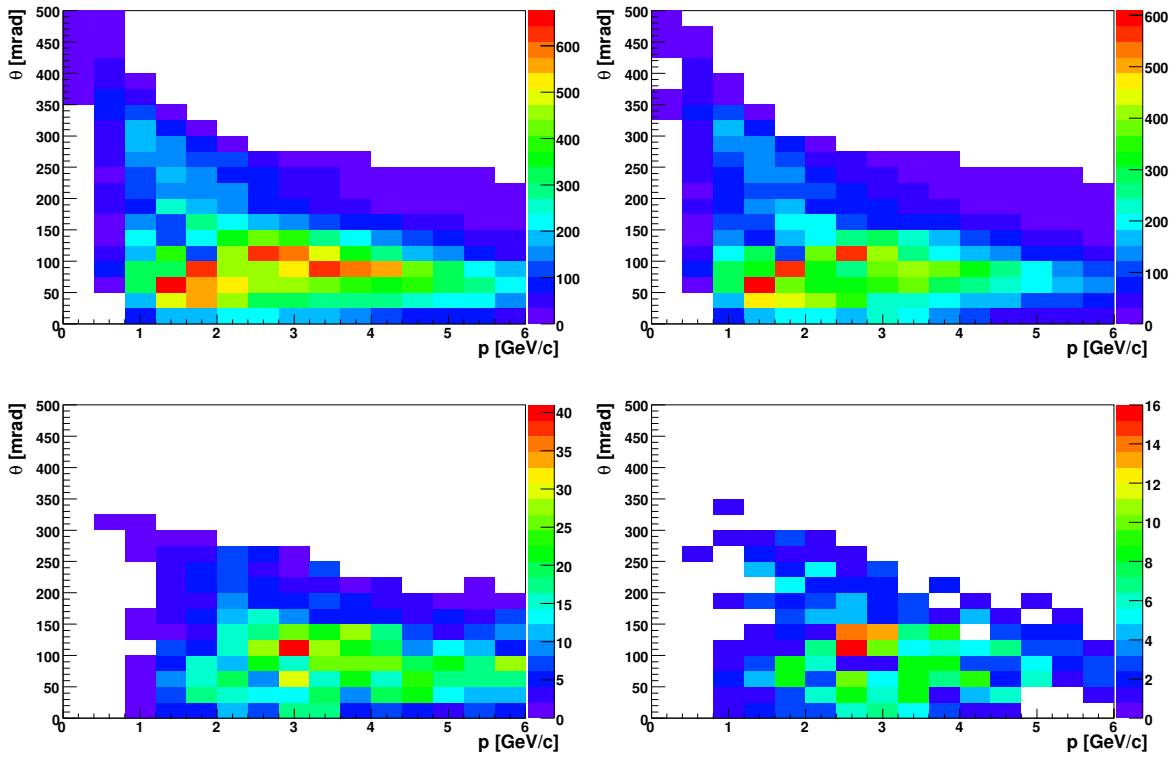

Figure 32: Momenta, p, versus polar angle, θ, for π^+ (*top-left*), π^- (*top-right*), K^+ (*bottom-left*) and K^- (*bottom-right*) identified by the combined dE/dx and *tof* measurements.

The azimuthal angle distribution, ϕ, for negatively charged tracks that reach the ToF-F is shown in Fig. 33 (left). The angle ϕ is defined to start at 0 along the positive x-axis direction (see the definition shown in the top-left corner of Fig. 1). The detector's geometrical acceptance is such that the distribution is peaked around $\phi = 0°$ and $\phi = 180°$ with a width of approximately 30°. The asymmetry in the distribution is due to the different track content of each peak: the peak at $\phi = 180°$ is populated by negatively charged right-side tracks (ratio of p_x momentum component over charge $p_x/Q > 0$), while the peak centered around $\phi = 0°$ is populated by negatively charged wrong-side tracks ($p_x/Q < 0$). Selection of tracks in the flat acceptance region ($\Delta\phi = 30°$ at the peak mean values) results in uniform acceptance in the whole T2K

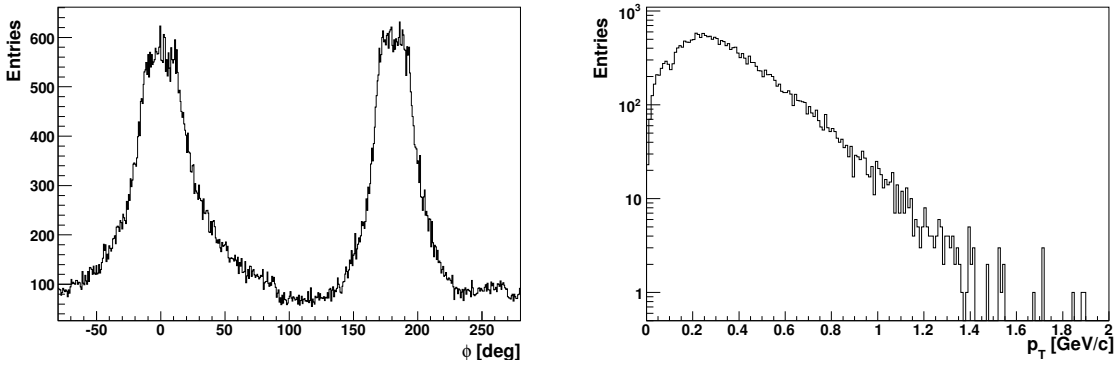

Figure 33: Negatively charged particles that reach the ToF-F: *Left:* Azimuthal angle (ϕ) distribution. *Right:* p_T distribution within the azimuthal angle wedges, $\Delta\phi = 30°$, centered at the peak mean values.

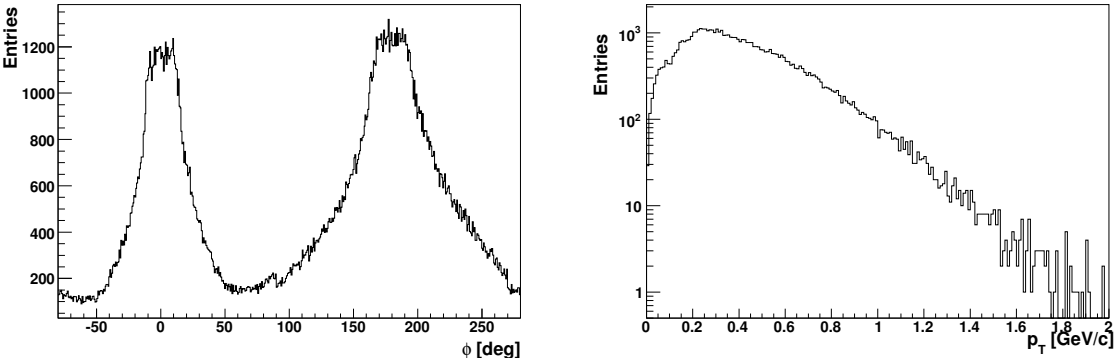

Figure 34: Positively charged particles that reach the ToF-F: *Left:* Azimuthal angle (ϕ) distribution. *Right:* p_T distribution within the azimuthal angle wedges, $\Delta\phi = 30°$, centered at the peak mean values.

$p - \theta$ phase space (see subsection 9.2).

A raw p_T distribution for negatively charged tracks within the azimuthal angle wedges, $\Delta\phi = 30°$, centered at the the peak mean values is shown in Fig. 33 (right). Although the spectrum is not corrected, fitting the data with an exponential p_T dependence yields a negative slope of about 6 $(\mathrm{GeV/c})^{-1}$ which is in agreement with the common parametrization of charged pion production [25, 26]. Similar distributions for positively charged tracks are presented in Fig. 34.

9 Simulation and Corrections

The raw spectra of identified hadrons discussed above still have to be corrected for geometrical acceptance, detector and tracking inefficiencies, event and track selection cuts as well as background contamination by use of the NA61 Monte Carlo simulation. The corresponding software and selected examples of the acceptance studies are presented in this section.

9.1 MC simulation

The NA61 simulation chain inherits from the software developed for the NA49 experiment. The chain is interfaced to GEANT 3.21 [23] for the particle propagation through the detector geometry and uses a model based input (VENUS 4.12 generator [24]) for the primary kinematics. The TPC digitization is performed by a dedicated plug-in during the reconstruction. Monte Carlo events are produced in the same format as raw data so that both are reconstructed with the same chain.

The NA61 simulation chain comprises several packages:

- **Event generation:** VENUS is used by default. Intrinsic generators (single or multi-pid flat phase space, real like event generators) are used as well for specific studies. External input may also be used if provided in the required ASCII format.

- **Propagation:** GEANT 3.21 propagates the particles through the whole NA61 geometry and accounts for secondary interactions and physics processes (decay, energy loss, multiple scattering, etc).

- **Format conversion:** the G2DS_NA61 package provides the conversion from zebra output (GEANT) to the DSPACK format which is used in the overall framework of the NA61 software.

- **Digitization:** the digitization of the NA61 TPCs is performed by a dedicated package (MTSIM). Energy loss from GEANT output is converted into ADC spectra and Monte Carlo data are packed in the same format as raw data. This package also performs simulation of distortions such as ExB distortions.

- **Embedding:** this package allows to merge raw data with Monte Carlo data prior to reconstruction.

- **Reconstruction:** Monte Carlo data are reconstructed with the chain used to process raw data. The chain calls different clients (cluster finding, pattern recognition, track merging and fitting, etc.) including correction of distortions applied to MC data.

The NA61 simulation chain includes new geometry volumes compared to the NA49 experimental set-up. This is in particular the case for the new forward time-of-flight wall that was built and installed to cover the NA61 physics needs for the T2K experiment.

9.2 Examples of NA61 acceptance studies

Monte Carlo studies have been performed to understand the geometrical acceptance in the region required by the T2K physics needs. Several examples are presented below.

For the study of the ToF geometrical acceptance up to 4 GeV/c and 400 mrad the momentum-angle (angle between the track and the beam axis) phase space was divided into 800 bins of 100 MeV/c and 20 mrad respectively. Each bin is normalized to 100 tracks. Due to the detector symmetry, studying only positive tracks is enough to understand the acceptance over the whole phase space.

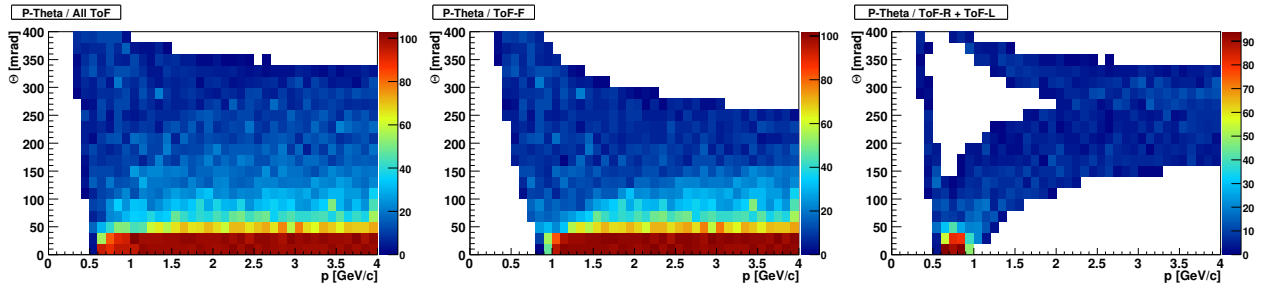

Figure 35: Acceptance for positive tracks within the full π azimuthal angle, requiring a time-of-flight signal for all ToF walls (left), ToF-F (middle), ToF-L/R walls (right).

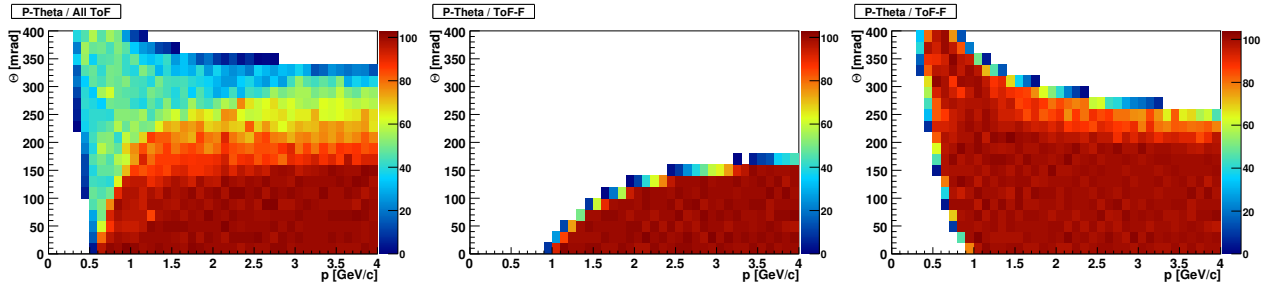

Figure 36: Acceptance for positive tracks within the selected azimuthal angle wedges of $\Delta\phi = 30°$ requiring a time-of-flight signal. Left: all ToF walls and two $\Delta\phi$ wedges centered at $\phi = 0°$ and $\phi = 180°$, middle: ToF-F and the $\Delta\phi$ wedge centered at $\phi = 0°$, right: ToF-F and the $\Delta\phi$ wedge centered at $\phi = 180°$.

As can be seen from Fig. 35, introduction of the ToF-F detector was necessary in order to to fill acceptance holes in the required T2K phase space. The combination of the three ToF walls covers completely the T2K phase space.

The NA61 detector geometry is not 2π symmetric in the plane transverse to the beam axis. In particular, the ToF acceptance is mostly limited to particles emitted in the azimuthal wedges

of $\Delta\phi = 30^\circ$ centered at the horizontal plane (see Fig. 33, left). The geometrical acceptance within the azimuthal wedges is shown in Fig. 36, which demonstrates that a significant region of the phase space relevant for T2K is covered by uniform acceptance of close to 100%.

10 Summary

The main goals of the 2007 NA61/SHINE run were reached, namely:

- the NA61/SHINE apparatus, including the new ToF-F system, was run successfully and detector prototypes were installed and tested.
- pilot physics data on interactions of 31 GeV/c protons on the thin and T2K replica carbon targets were registered.
- The NA61 reconstruction and simulation software has been set up and used successfully to process the events from the pilot run.
- Calibrations of all detector components have been performed successfully and preliminary uncorrected identified particle spectra have been obtained.
- High quality of track reconstruction and particle identification similar to NA49 has been achieved.
- The data as well as new detailed simulations confirm that the NA61 detector acceptance and particle identification capabilities cover the phase space required by the T2K experiment. The new ToF-F system extends significantly the NA49 PID acceptance in the domain relevant for the T2K measurements.
- A preliminary result of $\sigma_{inel} = 254.7 \pm 1.0$ (stat) mb was obtained for the total inelastic p+C cross section at 31 GeV/c.

Corrected spectra of identified pions, kaons and protons produced in 31 GeV/c p+C interactions will soon become available.

Acknowledgements: This work was supported by the Virtual Institute VI-146 of Helmholtz Gemeinschaft, Germany, Korea Research Foundation (KRF-2007-313-C00175), the Hungarian Scientific Research Fund (OTKA 68506), the Polish Ministry of Science and Higher Education (N N202 3956 33), the Federal Agency of Education of the Ministry of Education and Science of Russian Federation (grant RNP 2.2.2.2.1547), the Russian Foundation for Basic Research (grant 08-02-00018), the Ministry of Education, Culture, Sports, Science and Technology, Japan, Grant-in-Aid for Scientific Research (18071005, 19034011, 19740162), the Swiss Nationalfonds Foundation 200020-117913 / 1 and ETH Reseach Grant TH-01 07-3.

References

[1] N. Antoniou *et al.* [NA61 Collaboration], CERN-SPSC-2006-034.

[2] N. Antoniou *et al.* [NA61 Collaboration], CERN-SPSC-2007-004.

[3] N. Abgrall *et al.* [NA61 Collaboration], CERN-SPSC-2007-019.

[4] S. Afanasev *et al.* [NA49 Collaboration], Nucl. Instrum. Meth. A **430**, 210 (1999).

[5] Y. Fujii, NIM A453, 237 (2000).

[6] `http://jnusrv01.kek.jp/public/t2k/`

[7] V. Blobel, MILLEPEDE: Linear Least Squares Fits with a Large Number of Parameters, `http://www.desy.de/~blobel/mptalks.html`

[8] F. Bergsma, CERN, private communication.

[9] C. Alt *et al.*, "Inclusive production of $\pi^{\pm}$ in p+p collisions at 158 GeV/c beam momentum", Eur. Phys. J. **C45**, 343 (2006).

[10] R. Brun et al., ROOT: An Object-Oriented Data Analysis Framework, `http://root.cern.ch`

[11] A. Sadovsky, "Investigation of K^+ meson production in C+C collisions at 2 A GeV with HADES", Ph.D. thesis, TU Dresden, FZD-464 2007, ISSN 1437-322X, (2007).

[12] T. Solovyeva, "Development of a selection method for one dimensonal distributions and its application for the quality control of the experimental data from the HADES experiment", diploma thesis (in Russian) unpublished, MEPHI (2008).

[13] R. Zybert and P. Buncic, "DSPACK: Object manager for high energy physics", Proceedings of Computing in High Energy Physics, Rio de Janeiro, 1995, 345-348

[14] The Standard Template Library, www.sgi.com/tech/stl

[15] S. Agostinelli *et al.* [GEANT4 Collaboration], "GEANT4: A simulation toolkit," Nucl. Instrum. Meth. A **506**, 250 (2003).

[16] Bellettini *et al.*, "Proton-nuclei cross section at 20 GeV", Nucl. Phys. 79 (1966) 609-624.

[17] S. P. Denisov *et al.*, "Absorption cross-sections for π, K, p and $\overline{p}$ on complex nuclei in the 6-GeV/c to 60-GeV/c momentum range", Nucl. Phys. B **61**, 62 (1973).

[18] A. S. Carroll *et al.*, "Absorption cross-sections of $\pi^{\pm}$, $K^{\pm}$, p and $\overline{p}$ on nuclei between 60 and 280 GeV/c", Phys. Lett. B **80**, 319 (1979).

[19] D. S. Ayres *et al.* [Fermilab Single Arm Spectrometer Group], "$\pi^{\pm}p$, $K^{\pm}p$, pp and $\overline{p}p$ elastic scattering from 50 to 175 GeV/c," Phys. Rev. D **15**, 3105 (1977).

[20] K. Levenberg, "A Method for the Solution of Certain Non-linear Problems in Least Squares", Quarterly of Applied Mathematics 2(2), 164, (1944).
D.W. Marquardt, "An Algorithm for the Least-Squares Estimation of Nonlinear Parameters", SIAM Journal of Applied Mathematics 11(2), 431, (1963).

[21] J. Podolanski and R. Armenteros, Philos. Mag. **45**, 13 (1954).

[22] C. Alt *et al.* [NA49 Collaboration], "Energy dependence of Lambda and Xi production in central Pb+Pb collisions at the CERN-SPS," arXiv:0804.3770 [nucl-ex].

[23] `http://wwwasdoc.web.cern.ch/wwwasdoc/geant/geantall.html`

[24] K. Werner, Phys. Rep. **87**, 232 (1993).

[25] S. R. Blattnig *et al.*, Phys. Rep. D**62**, 094030 (1977).

[26] G. D. Badhwar *et al.*, Phys. Rep. D**15**, 820 (1977).